September 30, 2010

CCN 222202
NRC Project #0748

U.S. Nuclear Regulatory Commission
Attention: Document Control Desk
Washington, D.C. 20555

SUBJECT: Contract No. DE-AC07-05ID14517 – Next Generation Nuclear Plant Project – Responses to Request for Information – Response to Questions about the Applicability of the Advanced Gas Reactor Test Results to Next Generation Nuclear Plant Project Fuel – NRC Project #0748

Consistent with the actions identified in *"NGNP Licensing Strategy – Report to Congress,"* dated August 2008, the purpose of this letter is to submit the subject Next Generation Nuclear Plant (NGNP) Project responses to NRC's Request for Information regarding TRISO fuel performance transmitted via e -mail dated April 22, 2010.

The NRC licensing process encourages early interactions to identify and resolve policy, regulatory, and key technical issues related to the proposed facility. We believe conducting effective interactions with the NRC is a critical part of the NGNP licensing strategy since the early resolution of issues can significantly improve the preparation of an acceptable license application, its subsequent review schedule, and ultimately, deployment of the NGNP.

In conjunction with the irradiation of the Advanced Gas Reactor (AGR-1) test fuel in the Advanced Test Reactor (ATR) at Idaho National Laboratory (INL), two issues were raised by the NRC concerning fuel behavior and burnup characteristics. These issues are as follows:

Issue 1: Diffusion through intact TRISO coatings data during irradiation tests compared to predicted values from modeling codes.

Issue 2: Fission product buildup in AGR-1 test samples, compare those anticipated for HTGR fuel.

The NGNP responses to these issues are provided in Enclosure 1.

Following NRC Staff review of these responses, NGNP would welcome appropriate dialogue regarding these issues, including follow-on questions or requests for additional information.

D080
NRO

If you have any questions regarding this submittal, please contact me at (208) 526-6063 or Jim Kinsey, Director, NGNP Regulatory Affairs at (208) 526-6882.

Sincerely,

Greg Gibbs, Project Director
Next Generation Nuclear Plant Project

PJ:CN

Enclosure:

1. TEV-1022, Rev. 1, Idaho National Laboratory, Technical Evaluation Study, "*Response to Questions about the Applicability of the AGR Test Results to NGNP Fuel*," September 9, 2010.

cc:

DOE-HQ
T. J. O'Connor
C. J. Sink
J. Zamore

DOE-ID
M. L. Adams, (w/o Enc.)
C. P. Fineman
R. V. Furstenau
A. J. Kraupp, (w/o Enc.)
S. M. Olson, (w/o Enc.)

INL
J. Alvarez, (w/o Enc.)
A. Clark, (w/o Enc.)
J. J. Grossenbacher, (w/o Enc.)
D. J. Hill, (w/o Enc.)
L. A. Sehlke, (w/o Enc.)

NRC
S. Basu
M. E. Mayfield
W. D. Reckley
J. F. Williams
T. Zaki

Document ID: TEV-1022
Revision ID: 1
Effective Date: 09/30/10

## Technical Evaluation Study

## Project No. 23841

# Response to Questions about the Applicability of the AGR Test Results to NGNP Fuel

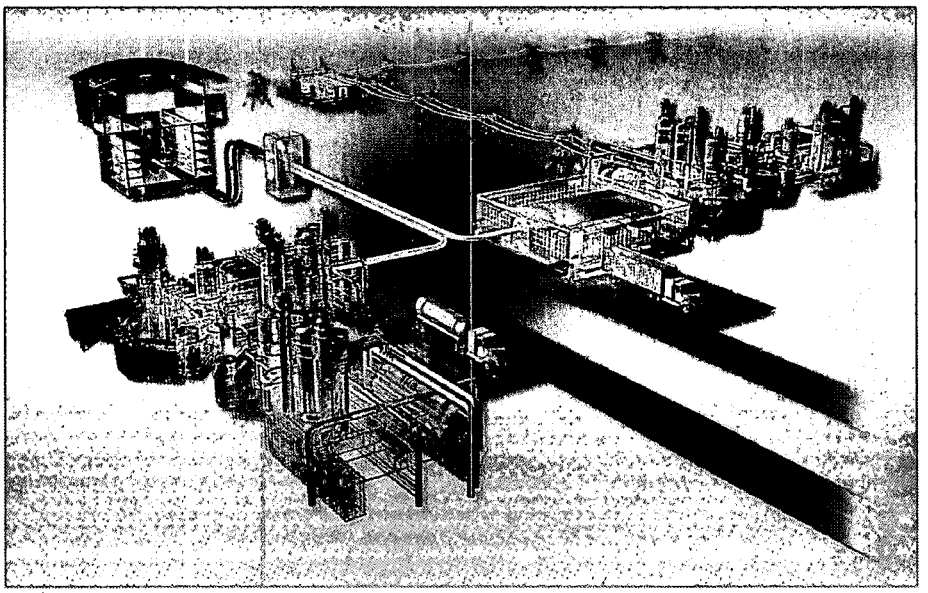

The INL is a
U.S. Department of Energy
National Laboratory
operated by
Battelle Energy Alliance

INL
Idaho National Laboratory

Idaho National Laboratory

| RESPONSE TO QUESTIONS ABOUT THE APPLICABILITY OF THE AGR TEST RESULTS TO NGNP FUEL | Identifier: TEV-1022<br>Revision: 1<br>Effective Date: 09/30/10 | Page: 1 of 42 |
|---|---|---|

| NGNP Project | Technical Evaluation Study (TEV) | eCR Number: 585486 |
|---|---|---|

## Signatures

| Signature and Typed or Printed Name | Signature Code | Date (mm/dd/yyyy) | Organization/Discipline |
|---|---|---|---|
| John T. Maki | P | 9-30-10 | Fuel Modeling and Simulation |
| James W. Sterbentz | P | 9/30/2010 | Reactor Physics Analysis and Design |
| Hans D. Gougar | A | 9/30/2010 | VHTR TDO Technical Deputy Director |
| for David A. Petti | C | 9/30/2010 | VHTR TDO Director |

**P** For Preparer of the document.

**A** For Approval: This is for non-owner approvals that may be required as directed by a given program or project. This signature may not be applicable for all uses of this form.

**C** For documented review and concurrence.

**Note:** Applicable QLD: REC-000169

## REVISION LOG

| Rev. | Date | Affected Pages | Revision Description |
|---|---|---|---|
| 0 | 09/09/10 | All | Newly issued document |
| 1 | 09/30/10 | 6,8,13,24 | Minor edits |
| | | | |
| | | | |
| | | | |
| | | | |
| | | | |
| | | | |
| | | | |
| | | | |
| | | | |
| | | | |
| | | | |

## CONTENTS

1. INTRODUCTION ..... 4

1.1 Description of the System ..... 4

1.2 Issue #1 - Diffusion through Intact TRISO Coatings During Irradiation ..... 5

1.3 Issue #2 – Fission rate and fission concentration buildup in AGR-1 test samples ..... 5

1.4 Acronyms ..... 5

2. Analysis and Issue Resolution ..... 6

2.1 Fission Product Diffusion under Irradiation and at High Temperatures ..... 6

2.2 Fission Concentration and Fission Product Buildup ..... 8

2.2.1 Neutron Spectra ..... 8
2.2.2 MHR Fuel Characteristics ..... 13
2.2.3 AGR-1 Fuel Characteristics ..... 17
2.2.4 Summary Comparison of the AGR-1 and the prismatic MHR TRISO Fuel Burnup Characteristics ..... 24
2.2.5 Pebble Bed HTGR Burnup Characteristics ..... 27

3. SUMMARY ..... 38

# 1. INTRODUCTION

In conjunction with the irradiation of the Advanced Gas Reactor (AGR)-1 test fuel in the Advanced Test Reactor (ATR) at Idaho National Laboratory (INL), two issues were raised by the Nuclear Regulatory Commission (NRC) in a query (see Appendix A) concerning fuel behavior and burnup characteristics. These issues are addressed in this Technical Evaluation, which has the following objectives:

- Confirm that irradiation-driven diffusion will be captured properly in the effective diffusion coefficients obtained from AGR fuel test data so that prediction of fission product transport using fuel performance modeling codes, such as PARFUME, will be conservative.

- Confirm that the total number of fissions and the resulting buildup of fission products that affect fuel performance in the AGR-1 test are comparable to those anticipated for HTGR fuel. (Other AGR tests will not achieve this level of burnup.)

## 1.1 Description of the System

The AGR-1 fuel test was comprised of multiple stacks of fueled compacts loaded into six independently controlled and monitored capsules assembled into a test train that were irradiated in the ATR core. The test is designed to investigate the performance of the tri-isotopic (TRISO) fuel under irradiation and temperature conditions, specifically with regard to fission product transport, TRISO layer stability, and isotopic burnup. The release of fission products during post-irradiation heat-up tests is a function of particle-coating failures and diffusion through intact layers during both irradiation and high temperature testing. Data from these tests will be used to develop fission product transport models in codes such as PARFUME; therefore, it is important that the effective diffusion coefficients derived from the data reflect the diffusion mechanisms anticipated in the reactor.

TRISO fuel performance is also strongly affected by the concentrations of fission products such as silver and palladium. These concentrations are dependent upon the fuel isotopes, thus the rate of formation changes with burnup as plutonium builds in and uranium burns out. The rate of plutonium build-up in the fuel is a strong function of the spectrum. As the AGR-1 test spectrum may differ from the NGNP spectrum, it is important that the final plutonium and fission concentrations in the AGR-1 test are comparable to those anticipated in NGNP fuel.

The complete letter of inquiry raising these issues is included as an Appendix. The letter provides additional background information as the context for the

query. The issues are provided here but the background information is not repeated.

### 1.2 Issue #1 - Diffusion through Intact TRISO Coatings During Irradiation

Metallic fission product (e.g., cesium) release data obtained from accident heat-up simulation tests are used for predicting metallic fission product diffusion coefficients for the fuel temperatures associated with a core heat-up accident. Because these heat-up tests are conducted as part of post-irradiation testing, they do not address any diffusion-related phenomena that are present during irradiation and absent afterward. The additional use of such post-irradiation heat-up data as "margin data" for predicting fission product diffusion during irradiation at operating temperatures above those addressed by the fuel qualification irradiations, could therefore be non-conservative. How can AGR test data inform or validate model predictions of fission product diffusion under irradiation vs. unirradiated conditions?

### 1.3 Issue #2 – Fission rate and fission concentration buildup in AGR-1 test samples

For (a) a reference HTGR design as well as (b) the recently completed AGR-1 and subsequent TRISO fuel irradiations in the ATR, what are the calculated quantities, as functions of total burnup and irradiation time, of the following quantities?

i. Concentrations of fissionable nuclides that contribute significantly to total fuel burnup (e.g., U-235, U-238, Pu-239, Pu-241) and associated nuclide-specific fission rates and burnup fractions,

ii. Concentrations of chemical elements that can potentially affect TRISO fuel performance, including palladium, rare earths, and silver.

The HTGR spectra and burnup calculations should be realistic rather than conservative. The spectra and therefore the transmutation rates will vary as a function of core position due changes in temperature, burnup, and surrounding composition. The HTGR results for the concentrations of actinides and fission products will therefore be approximate but should be of the same order of magnitude as those attained in the AGR-1 irradiations.

### 1.4 Acronyms

AGR Advanced Gas Reactor

ATR Advanced Test Reactor

BOL beginning of life

| | |
|---|---|
| EOL | end of life |
| FIMA | fissions per initial (heavy) metal atom |
| GA | General Atomics |
| HEU | high-enriched uranium |
| HTGR | high temperature gas-cooled reactor |
| INL | Idaho National Laboratory |
| LEU | low-enriched uranium |
| MCNP | Monte Carlo N-Particle Transport Code |
| MHR | modular helium reactor |
| MTR | metals test reactor |
| NGNP | Next Generation Nuclear Plant |
| NRC | Nuclear Regulatory Commission |
| PBR | pebble bed reactor |
| PMBR | pebble bed modular reactor |
| TRISO | tri-isotropic (fuel) |
| VHTR | very high temperature reactor |

# 2. Analysis and Issue Resolution

## 2.1 Fission Product Diffusion under Irradiation and at High Temperatures

The effect of neutron flux on enhancing transport of vacancies in ceramics (and thus fission products because diffusion in ceramics is via vacancy movement) has been seen before in nuclear fuel systems.[1,2] These irradiation induced athermal (independent of temperature) and irradiation enhanced vacancy diffusion mechanisms are captured in fission gas release models in $UO_2$ and are currently used in PARFUME (Figure 1) to estimate fission gas release from kernels to calculate internal gas pressure in TRISO fuel particles. These irradiation enhanced

1 Matzke, Hj (1983) "Radiation Enhanced Diffusion in UO2 and (U,Pu)O2," Radiation Effects and Defects in Solids, 75, Issue 1-4, August 1983, p. 317-325.

2 Turnbull, J. A., et. al, (1982) "The Diffusion Coefficients of Gaseous and Volatile Species during Irradiation of Uranium Dioxide," Journal of Nuclear Materials, 107, Issues 2-3, June 1982, p. 168-184.

mechanisms tend to dominate in $UO_2$ at low temperatures below 1000°C. At higher temperatures, traditional intrinsic diffusion mechanisms (where thermal energy is available to promote diffusion in a material in a concentration gradient) tend to dominate. At intermediate temperatures, both intrinsic and irradiation enhanced mechanisms can contribute to fission product transport. In $UO_2$, the Turnbull model[2] would predict a cross-over in these mechanisms at about 1200°C. Less is known about the mechanisms responsible for fission product transport in SiC, but ion irradiation enhanced diffusion of impurities in semiconductors has been studied.[3]

To accurately model fission product transport in TRISO coated particle fuel under high temperature irradiation, use of "effective" diffusion coefficients for the kernel and coatings (as presented in the IAEA TECDOC 978[4]) obtained from post-irradiation heating tests is not recommended because those coefficients do not consider the irradiation effects, either implicitly or explicitly. The AGR program will obtain "effective" diffusion coefficients in kernels and coatings under irradiation from the AGR-1 experiment , possibly from the AGR-2 experiment for capsules experiencing no particle failures, and the AGR-7 experiment in which higher temperatures and irradiation are planned. Careful post-irradiation examination (PIE) measurements of fission product concentrations in the capsule components, combined with knowledge of release from uranium contamination, could provide an estimate of effective diffusion coefficients under irradiation. Such effective diffusion coefficients estimated from this data will implicitly include both intrinsic and irradiation enhanced diffusion. Subsequent post-irradiation heating tests will yield effective diffusion coefficients for accident safety evaluations. These coefficients will reflect intrinsic diffusion (from particles and uranium contamination) as no neutron flux will be present. Irradiation enhanced diffusion effects may then be "isolated" from the combined datasets by subtracting the intrinsic diffusivity values (obtained from safety heating tests) from the irradiation condition diffusivity values (obtained from irradiation test PIE). Considering the complexity of the measurements, multiple material compositions encountered in the diffusion path length, the presence of uranium contamination, and the expected low diffusivity for most fission products in SiC at typical irradiation temperatures, there will be a large uncertainty in this isolated enhanced irradiation diffusion evaluation.

First principles computation material science modeling will also provide some insight into the different mechanisms of transport in SiC and pyrolytic carbon (PyC), which is why the Next Generation Nuclear Plant (NGNP) has sponsored some of this research in the universities. Following the conclusion of these research grants in the next few years, follow-on simple experiments (including

3. Schmidt, P. F., D.V. McCaughan and and R. A. Kushner, "Problems in the Analysis of Semiconductor Device Materials Exposed to Ionizing Radiation," Proceedings of IEEE, 74, No. 9, September 1974, p. 1220-1223

4 International Atomic Energy Agency (1997) http://www.iaea.org/inisnkm/nkm/aws/htgr/abstracts/abst_29009817.html, Web page accessed August 5, 2010.

potential irradiations) may be conducted to validate the results of the research, depending on the results of the modeling.

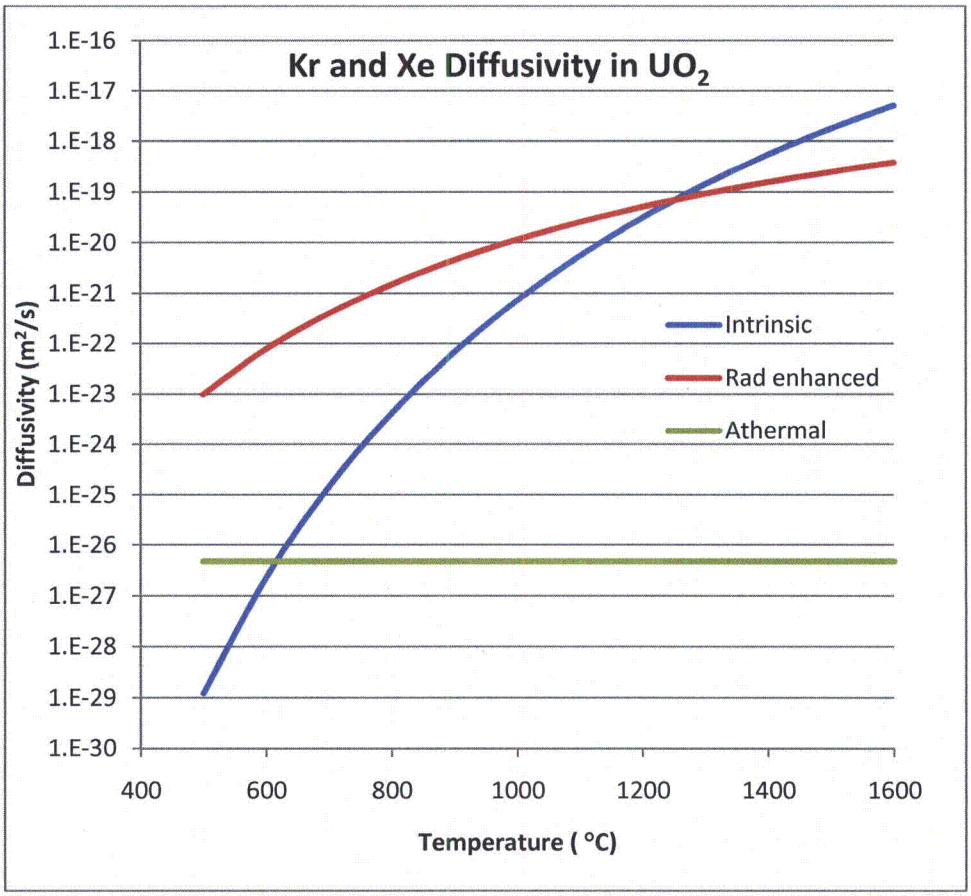


Figure 1. Kr and Xe diffusivity in $UO_2$ as a function of temperature [Turnbull - see footnote 2 on page 6].

## 2.2 Fission Concentration and Fission Product Buildup

### 2.2.1 Neutron Spectra

Figure 2 shows the neutron energy spectra in an AGR-1 fuel compact as a function of the 13 ATR burnup cycles that comprise the AGR-1 experiment. This particular fuel compact resides in the AGR-1 test assembly in capsule 4 (stack 1) which is just above the ATR core midplane and in the maximum neutron irradiation flux zone (axially). These spectra were calculated with the Monte Carlo N-Particle Transport Code (MCNP5) code using the JMOCUP MCNP ATR

full-core model for the AGR-1 depletion calculation. It should be noted that the calculated neutron spectra in Figures 2-4 are normalized to one neutron.

Of particular interest in the spectral curves in Figure 2 is the position of the thermal neutron flux peak at approximately 0.09 eV, and the fact that the thermal flux tends to increase in magnitude with each progressive cycle, or increasing burnup. For example, the flux initially starts out with cycle 138B (lower black line) with a maximum magnitude of approximately 0.01 and by the 12$^{th}$ or 13$^{th}$ cycle reaches a magnitude of 0.03.

The increase in the thermal flux is due to the depletion of the burnable poison (B-10) in the borated graphite holder, and to a lesser extent due to the depletion of the hafnium isotopes in the shroud surrounding the AGR-1 capsules facing the core. The B-10 was specifically placed in the graphite holder to reduce the irradiation thermal flux and hence the fission rate in the AGR-1 fuel compacts. This was needed specifically for the first several ATR power cycles when the fresh TRISO particle fuel was most reactive. The partial-circumferential hafnium shroud was used to reduce the fission rates in the two compact fuel stacks facing the ATR core in order to help equalize the fission rates among all three stacks. As the B-10 and hafnium isotopes deplete over the course of the burnup cycles, the AGR-1 thermal flux tends to increase in magnitude. After approximately six cycles the spectrum begins to stabilize (Figure 2).

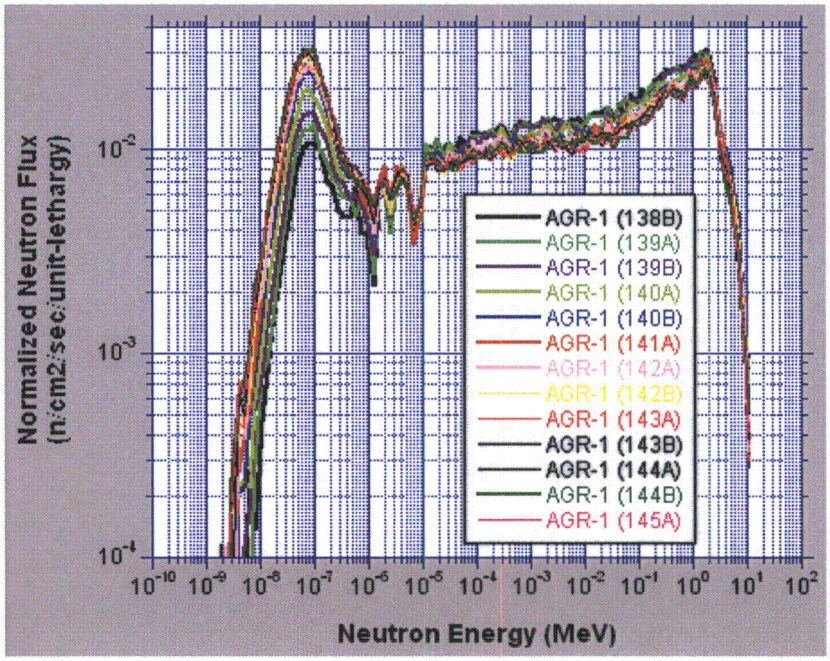


Figure 2. AGR-1 compact normalized neutron flux spectra as a function of ATR cycle (or burnup).

Figure 3 shows the neutron energy spectra for fuel compacts in each of the three active core annular rings of the General Atomics (GA) Modular Helium Reactor (MHR).[5] The MHR is a prismatic high temperature gas-cooled reactor with an annular active core design. The active core consists of fuel blocks in hexagonal rings 6, 7, and 8. Rings 1-5 comprise the inner graphite reflector and rings 9-11 the outer graphite reflector. The MHR core design serves as the NGNP baseline prismatic HTGR for the fuel burnup study here. Spectra in the MHR fuel rings are largely insensitive to burnup.

MHR neutron spectra are calculated using a 1/12-core MCNP5 model of the MHR core with a uniform compact fuel temperature of 1100 °C and surrounding block graphite at 927 °C. The block-average, uniform-temperature spectra show little difference between the three fueled rings, as one might expect, since local variations due to control rod, burnable poison, and reflector-core interface conditions not accounted for.

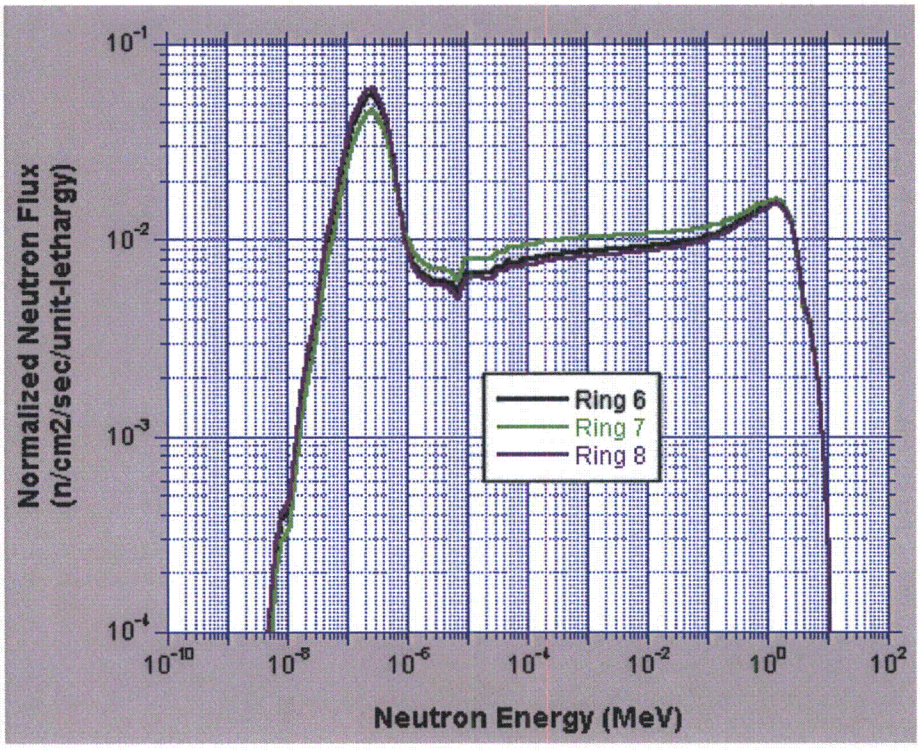


Figure 3. MHR compact neutron flux spectra for the three core annulus fuel element rings.

The MHR spectra in Figure 3 show the thermal neutron flux peak to be at approximately 0.3 eV, whereas, the AGR-1 thermal neutron flux peak was at approximately 0.09 eV (Figure 1). This means the MHR thermal neutron flux

5. GA Report 910720, Project No. 7658, General Atomics (1996) "Gas Turbine-Modular Helium reactor (GT-MHR) Conceptual Design Description Report," Revision 1, General Atomics, San Diego, CA (1996).

spectrum is a harder energy spectrum relative to the AGR-1 irradiation spectrum in ATR.

For comparison purposes, Figure 4 overlays the MHR (ring 6) spectrum with the AGR-1 beginning-of-life (Cycle 138B) and the end-of-life (Cycle 145A) spectrums. The energy difference in the thermal peaks is readily discernable. Plus, the MHR thermal flux is larger in magnitude relative to the AGR-1 spectra, although by the last cycle (cycle 145A), the AGR-1 thermal flux peak magnitude has increased by a factor of 3, and is now more comparable to the hot MHR thermal flux peak.

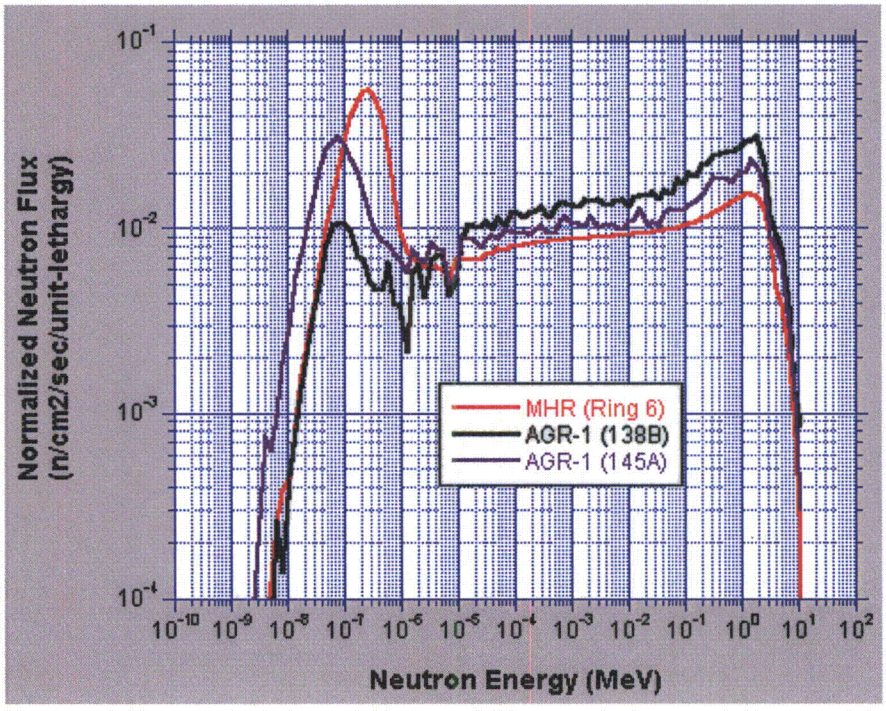


Figure 4. Comparison of the MHR (ring 6) and AGR-1 spectra.

One factor that does influence the MHR thermal neutron flux magnitude and peak energy is the temperature of the fuel and block graphite[6]. Increasing the fuel and graphite temperatures shifts the thermal neutron flux peak up in energy and increases the magnitude of the thermal flux as well. Figure 5 shows MHR flux spectrums for the two bounding sets of temperature conditions: (1) 1100 °C fuel and 927 °C graphite; and (2) 20 °C fuel with 20 °C graphite. These curves happen to be normalized to a 600 MW MHR power level (note here that the red curve corresponds to the MHR ring 6 spectra in Figures 3 and 4). In Figure 5, the 20 °C thermal neutron flux peak (cold) is shifted down in energy to 0.08 eV relative to

6 Sterbentz, James, W. (2008) "Calculated Neutron and Gamma-ray Spectra across the Prismatic Very High Temperature Reactor Core," 13th International Symposium on Reactor Dosimetry (ISRD-13), May 2008.

the 1100 °C case (hot) at 0.3 eV, and the magnitude is reduced by a factor of 2. It is not hard to visualize intermediate temperature spectrums between these two bounding temperature cases. Intermediate flux spectra could be representative of axial and radial locations in the MHR core where fuel and graphite temperatures might vary between the 20-1100 °C range depending on actual inlet gas temperature (~500 °C), outlet gas temperature (750-850 °C), and core power level (≤600 $MW_{th}$).

If one assumes fuel and graphite temperatures less than 1100 °C, these intermediate spectra would be softer than the 1100 °C spectrum and harder than the 20 °C spectrum, thus the actual AGR-1 spectra in the ATR lie between these two curves.

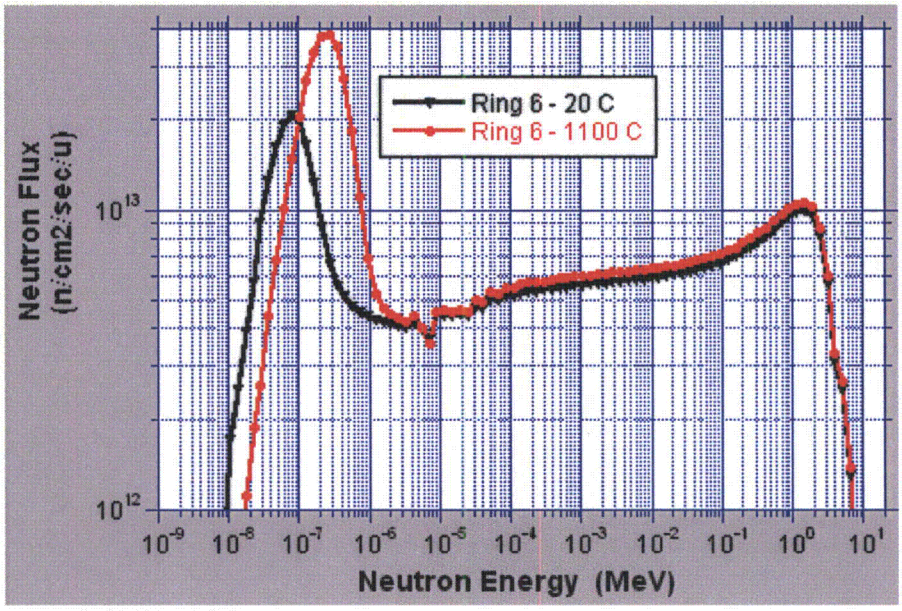


Figure 5. Effect of temperature on the MHR neutron spectra for two bounding temperature cases.

Spectral differences do however exist between the MHR and the AGR-1 irradiation test. The peak thermal flux energies and the magnitudes of the thermal neutron flux are different. In the MHR with an assumed core power level of 600 MW(thermal), the total neutron flux intensity ranges from approximately 1.2–2.0E+14 n/$cm^2$/sec. In the AGR-1 test near the ATR core midplane, the total neutron flux ranged from approximately 2.4–4.2E+14 n/$cm^2$/sec. The ATR irradiation flux was approximately double the total flux expected in the MHR active core. The factor of two larger total neutron flux in the AGR-1 test represents an acceleration factor of 2. An acceleration factor of 3 or less was deemed acceptable by AGR-1 test planners.

### 2.2.2 MHR Fuel Characteristics

There is currently no reference core design for the NGNP prismatic reactor and no official supporting burnup analysis. However, in order to perform a preliminary comparative fuel burnup study here between the AGR-1 test and a prismatic NGNP reactor, the General Atomics MHR will be used as the reference design for this study.

The ORIGEN2.2 code and an associated MHR standard fuel block model are used to perform a depletion calculation. Applicable neutron cross sections were obtained from a previous INL NGNP fuel depletion analysis[7] and fissile-particle, block, and burnup characteristics are borrowed from a recent core performance study performed by GA[8]. In this GA study, both a binary-particle (19.9 wt% U235 fissile-particle and 0.71 wt% U235 or natural uranium fertile-particle) and a single fissile-particle (15.5 wt% U235) are considered in the core design analyses. For the comparison here, only the 19.9 wt% U235 fissile-particle (UCO 350 μm kernel) from the binary-particle is considered, since the AGR-1 particle was also a 19.9 wt% fissile-particle (UCO 350 μm kernel). Also, in both cases, only the maximum burnup compacts in the MHR and AGR-1 are considered, i.e. those compacts with the highest burnup (GWD/MTU and % FIMA).

From the GA study[8], the maximum or peak burnup on the 19.9 wt% enriched fissile particle was 20.2 % FIMA. The peak burnup during the equilibrium cycles was estimated to be 19.7 % FIMA. Therefore, for the MHR burnup calculation here, the goal will be to achieve a peak burnup in the neighborhood of 19.7–20.2 % FIMA. This will then be in-line with the 19.8 % FIMA achieved by the maximum burnup compact in the AGR-1 test.

Modeling assumptions used in the MHR maximum compact burnup analysis include the following: (1) maximum or peak TRISO fissile-particle fuel burnup of 19.9 % FIMA (~191 GWD/MTU), (2) fissile-particle enrichment of 19.9 wt% U-235, (3) compact particle packing fraction of 30%, (4) 350 micron TRISO kernel diameter, (5) uranium block loading of about 981 grams U-235 and about 3,947 grams U-238,(6) 40-day burnup increments, and (7) constant average block power over the burnup duration (588kW/block).

**MHR Mass Isotopics**

Figure 6 shows the mass concentrations of U-235, U-236, U-238 and Pu-239, Pu-240, and Pu-241 as a function of burnup in gigawatt-days per metric ton of initial

---

[7] Sterbentz, James W., et al., "Reactor Physics Parametric and Depletion Studies in Support of TRISO Particle Fuel Specification for the Next Generation Nuclear Plant," INEEL/EXT-04-02331.

[8] GA Report No. 911184 (2009) "Final Report—NGNP Core Performance Analysis, Phase 2, Engineering Services for the Next Generation Nuclear Plant (NGNP) with Hydrogen Production," Revision 0, General Atomics, September 2009.

uranium (GWD/MTU). The y-axis is the specific mass, or the isotopic mass in grams divided by the corresponding initial amount of uranium (U-235 and U-238) at the beginning of the burnup. This was done in order to make a one-to-one comparison later with the corresponding AGR-1 maximum burnup characteristics in the following section.

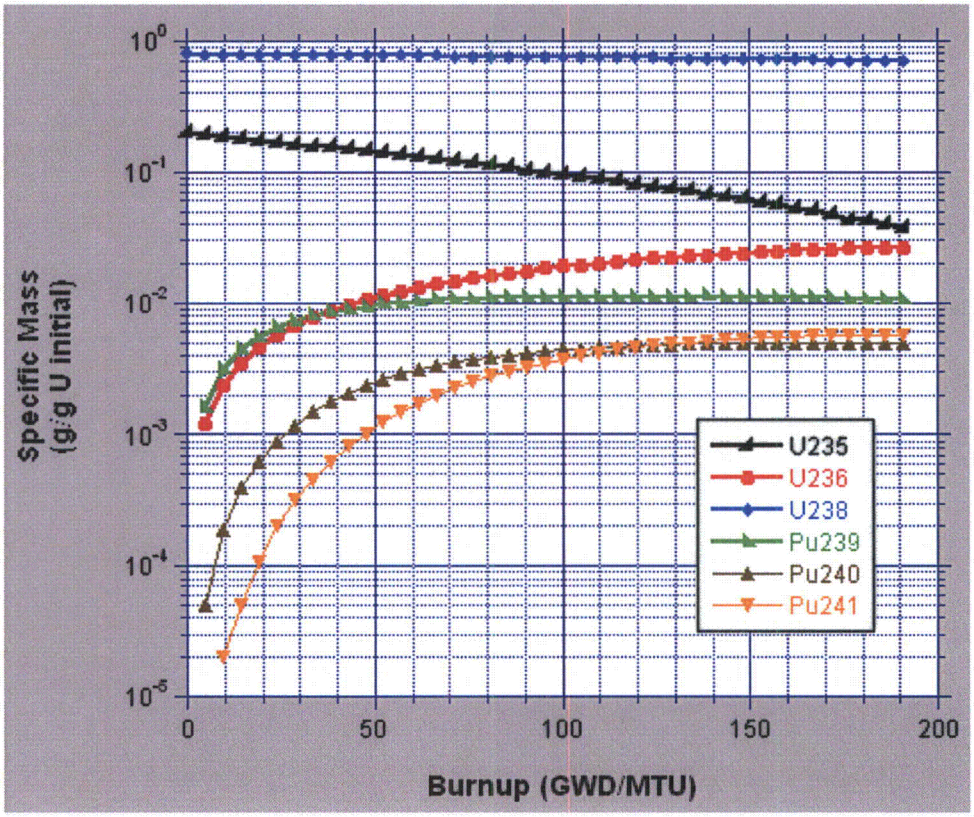


Figure 6. MHR fuel isotopic specific MASS as a function of burnup (GWD/MTU).

## MHR Fissions

Figure 7 shows the isotopic fissions per initial mass of uranium, or specific fissions (fissions/g U initial), as a function of burnup. Note that the plotted points in this figure are the total specific fissions in each 40-day burnup increment, and not the cumulative fissions which will be plotted later. Again the total fissions have been divided by the beginning-of-life mass of uranium (U-235 and U-238) in order to make a one-to-one comparison with the AGR-1 test fuel.

Table 1 gives the estimated specific fissions for U-235, U-236, U-238, Pu-239, Pu-240, and Pu-241 as a function of burnup (by 40-day increment). These are the same data plotted in Figure 7. Isotopic fission totals are given at the bottom of the table.

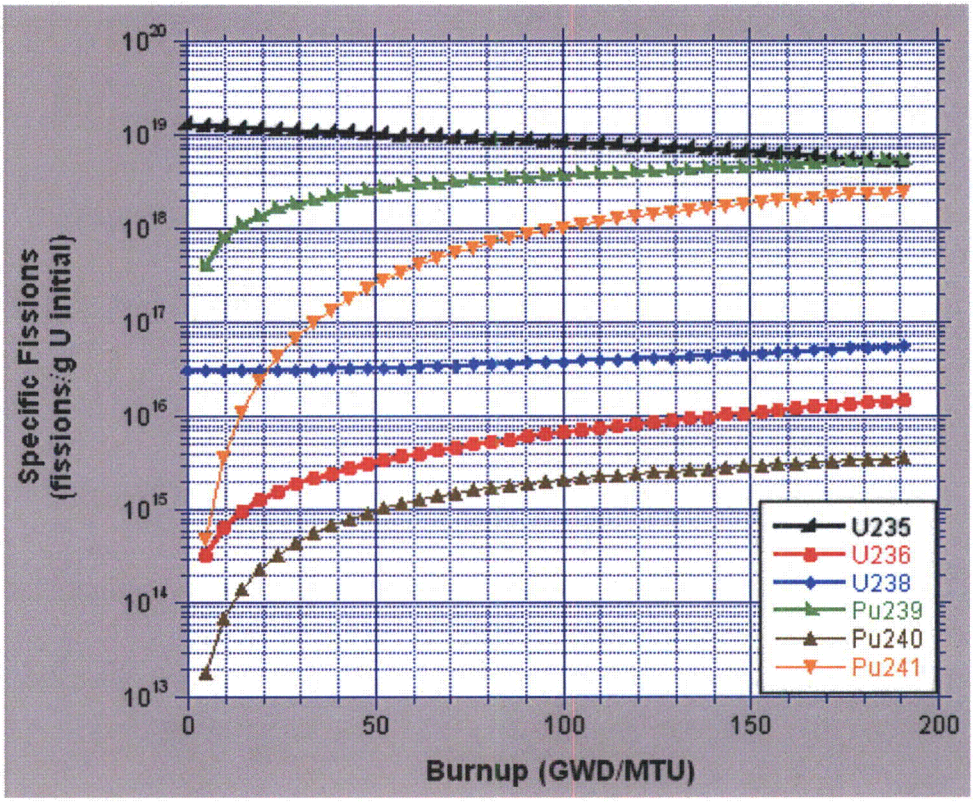


Figure 7. MHR fuel isotopic specific FISSIONS as a function of burnup (GWD/MTU).

Table 1. MHR estimated isotopic fissions (fissions/g uranium initial) as a function of burnup.

| Burnup (GWD/MTU) | U-235 | U-236 | U-238 | Pu-239 | Pu-240 | Pu-241 |
|---|---|---|---|---|---|---|
| 4.78 | 1.24E+19 | 3.32E+14 | 3.08E+16 | 4.00E+17 | 1.80E+13 | 4.83E+14 |
| 9.55 | 1.21E+19 | 6.52E+14 | 3.07E+16 | 7.76E+17 | 6.78E+13 | 3.56E+15 |
| 14.33 | 1.17E+19 | 9.63E+14 | 3.08E+16 | 1.10E+18 | 1.41E+14 | 1.10E+16 |
| 19.10 | 1.14E+19 | 1.27E+15 | 3.09E+16 | 1.38E+18 | 2.30E+14 | 2.40E+16 |
| 23.88 | 1.12E+19 | 1.57E+15 | 3.10E+16 | 1.63E+18 | 3.32E+14 | 4.30E+16 |
| 28.65 | 1.09E+19 | 1.88E+15 | 3.13E+16 | 1.85E+18 | 4.42E+14 | 6.84E+16 |
| 33.43 | 1.07E+19 | 2.18E+15 | 3.15E+16 | 2.04E+18 | 5.58E+14 | 1.00E+17 |
| 38.20 | 1.05E+19 | 2.48E+15 | 3.18E+16 | 2.22E+18 | 6.77E+14 | 1.38E+17 |
| 42.98 | 1.03E+19 | 2.79E+15 | 3.22E+16 | 2.38E+18 | 7.98E+14 | 1.82E+17 |
| 47.75 | 1.01E+19 | 3.10E+15 | 3.25E+16 | 2.52E+18 | 9.20E+14 | 2.32E+17 |
| 52.53 | 9.90E+18 | 3.41E+15 | 3.29E+16 | 2.65E+18 | 1.04E+15 | 2.88E+17 |
| 57.30 | 9.72E+18 | 3.72E+15 | 3.33E+16 | 2.77E+18 | 1.16E+15 | 3.47E+17 |
| 62.08 | 9.54E+18 | 4.04E+15 | 3.38E+16 | 2.89E+18 | 1.28E+15 | 4.12E+17 |
| 66.85 | 9.36E+18 | 4.37E+15 | 3.43E+16 | 2.99E+18 | 1.39E+15 | 4.80E+17 |
| 71.63 | 9.19E+18 | 4.70E+15 | 3.48E+16 | 3.09E+18 | 1.50E+15 | 5.51E+17 |
| 76.40 | 9.02E+18 | 5.03E+15 | 3.53E+16 | 3.19E+18 | 1.61E+15 | 6.25E+17 |
| 81.18 | 8.85E+18 | 5.37E+15 | 3.58E+16 | 3.28E+18 | 1.71E+15 | 7.01E+17 |
| 85.95 | 8.69E+18 | 5.71E+15 | 3.64E+16 | 3.37E+18 | 1.81E+15 | 7.79E+17 |
| 90.73 | 8.52E+18 | 6.06E+15 | 3.70E+16 | 3.45E+18 | 1.91E+15 | 8.58E+17 |
| 95.50 | 8.36E+18 | 6.42E+15 | 3.76E+16 | 3.54E+18 | 2.00E+15 | 9.38E+17 |
| 100.28 | 8.19E+18 | 6.78E+15 | 3.82E+16 | 3.62E+18 | 2.09E+15 | 1.02E+18 |
| 105.05 | 8.03E+18 | 7.15E+15 | 3.89E+16 | 3.70E+18 | 2.18E+15 | 1.10E+18 |
| 109.83 | 7.87E+18 | 7.52E+15 | 3.96E+16 | 3.78E+18 | 2.27E+15 | 1.18E+18 |
| 114.60 | 7.70E+18 | 7.91E+15 | 4.03E+16 | 3.86E+18 | 2.35E+15 | 1.26E+18 |
| 119.38 | 7.54E+18 | 8.29E+15 | 4.10E+16 | 3.95E+18 | 2.43E+15 | 1.34E+18 |
| 124.15 | 7.37E+18 | 8.69E+15 | 4.18E+16 | 4.03E+18 | 2.51E+15 | 1.42E+18 |
| 128.93 | 7.21E+18 | 9.09E+15 | 4.26E+16 | 4.11E+18 | 2.59E+15 | 1.50E+18 |
| 133.70 | 7.05E+18 | 9.51E+15 | 4.35E+16 | 4.20E+18 | 2.67E+15 | 1.58E+18 |
| 138.48 | 6.79E+18 | 9.80E+15 | 4.37E+16 | 4.40E+18 | 2.71E+15 | 1.63E+18 |
| 143.25 | 6.71E+18 | 1.03E+16 | 4.52E+16 | 4.38E+18 | 2.82E+15 | 1.73E+18 |
| 148.03 | 6.54E+18 | 1.08E+16 | 4.61E+16 | 4.47E+18 | 2.89E+15 | 1.80E+18 |
| 152.80 | 6.38E+18 | 1.12E+16 | 4.70E+16 | 4.56E+18 | 2.97E+15 | 1.87E+18 |
| 157.58 | 6.21E+18 | 1.17E+16 | 4.80E+16 | 4.66E+18 | 3.04E+15 | 1.95E+18 |
| 162.35 | 6.04E+18 | 1.21E+16 | 4.90E+16 | 4.76E+18 | 3.12E+15 | 2.02E+18 |
| 167.13 | 5.86E+18 | 1.26E+16 | 5.00E+16 | 4.86E+18 | 3.20E+15 | 2.09E+18 |
| 171.90 | 5.69E+18 | 1.30E+16 | 5.11E+16 | 4.96E+18 | 3.27E+15 | 2.16E+18 |
| 176.68 | 5.35E+18 | 1.38E+16 | 5.33E+16 | 5.18E+18 | 3.42E+15 | 2.28E+18 |
| 181.45 | 5.33E+18 | 1.40E+16 | 5.32E+16 | 5.18E+18 | 3.42E+15 | 2.29E+18 |
| 186.23 | 5.15E+18 | 1.44E+16 | 5.44E+16 | 5.29E+18 | 3.50E+15 | 2.36E+18 |
| 191.00 | 4.98E+18 | 1.49E+16 | 5.55E+16 | 5.40E+18 | 3.58E+15 | 2.43E+18 |
| TOTAL | 3.34E+20 | 2.80E+17 | 1.59E+18 | 1.37E+20 | 7.66E+16 | 4.18E+19 |

Figure 8 shows the MHR cumulative specific isotopic fissions as a function of burnup.

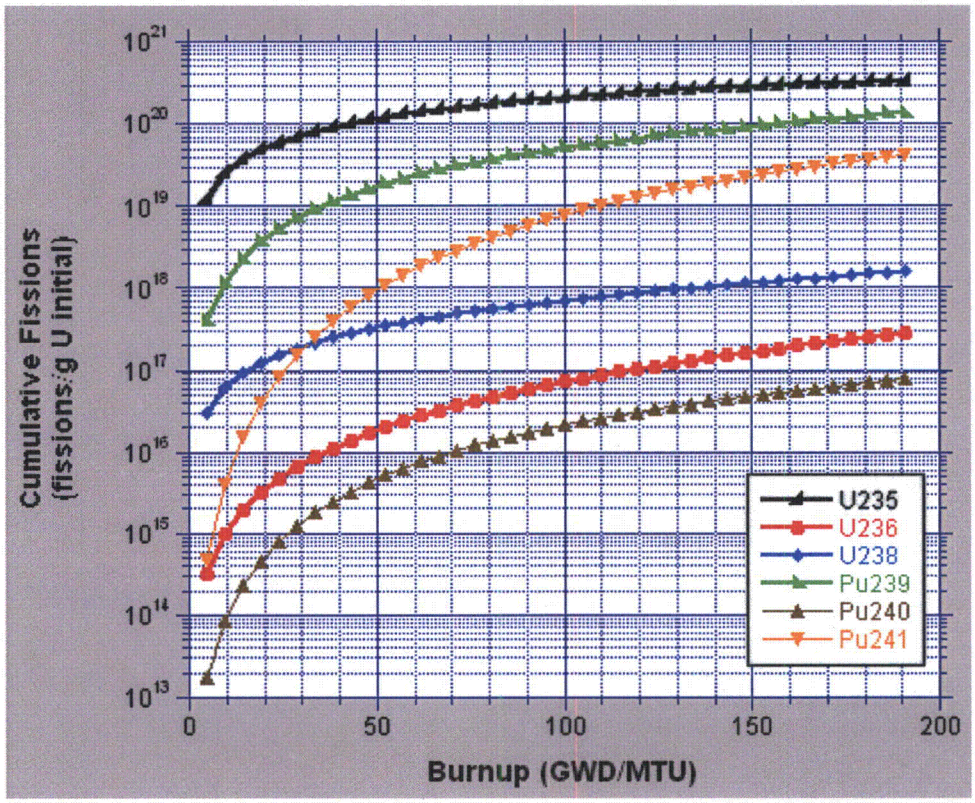


Figure 8. MHR cumulative specific FISSIONS as a function of burnup (GWD/MTU).

Table 2 gives the MHR cumulative specific isotopic fissions for U-235, U-236, U-238, Pu-239, Pu-240, and Pu-241 fissions as a function of burnup (GWD/MTU). These are the same data as plotted in Figure 8.

### 2.2.3 AGR-1 Fuel Characteristics

The AGR-1 test was comprised of 72 total fuel compacts. The 72 compacts were loaded into six capsules with 12 compacts per capsule. In the test assembly, capsule 1 was on the bottom and capsule 6 on the top. Situated in the ATR reactor core, the ATR core midplane was between capsules 3 and 4. Hence, compacts in capsules 3 and 4 experienced the highest burnups which resulted in the highest % FIMAs, or the percentage of the initial [heavy] metal atoms fissioned. In addition, these highest % FIMA compacts also experienced the highest burnup in terms of energy release per initial uranium mass, or burnup (GWD/MTU). The initial [heavy] metal atoms includes only U-235 and U-238 in the fresh compacts.

Table 2. Cumulative MHR estimated isotopic specific fissions (fissions/g uranium initial) as a function of burnup.

| Burnup (GWD/MTU) | U-235 | U-236 | U-238 | Pu-239 | Pu-240 | Pu-241 |
|---|---|---|---|---|---|---|
| 4.78 | 1.24E+19 | 3.32E+14 | 3.08E+16 | 4.00E+17 | 1.80E+13 | 4.83E+14 |
| 9.55 | 2.45E+19 | 9.84E+14 | 6.15E+16 | 1.18E+18 | 8.58E+13 | 4.05E+15 |
| 14.33 | 3.62E+19 | 1.95E+15 | 9.23E+16 | 2.28E+18 | 2.26E+14 | 1.51E+16 |
| 19.10 | 4.77E+19 | 3.22E+15 | 1.23E+17 | 3.66E+18 | 4.57E+14 | 3.90E+16 |
| 23.88 | 5.89E+19 | 4.79E+15 | 1.54E+17 | 5.28E+18 | 7.89E+14 | 8.20E+16 |
| 28.65 | 6.98E+19 | 6.67E+15 | 1.85E+17 | 7.13E+18 | 1.23E+15 | 1.50E+17 |
| 33.43 | 8.05E+19 | 8.84E+15 | 2.17E+17 | 9.17E+18 | 1.79E+15 | 2.51E+17 |
| 38.20 | 9.10E+19 | 1.13E+16 | 2.49E+17 | 1.14E+19 | 2.47E+15 | 3.89E+17 |
| 42.98 | 1.01E+20 | 1.41E+16 | 2.81E+17 | 1.38E+19 | 3.26E+15 | 5.71E+17 |
| 47.75 | 1.11E+20 | 1.72E+16 | 3.13E+17 | 1.63E+19 | 4.18E+15 | 8.04E+17 |
| 52.53 | 1.21E+20 | 2.06E+16 | 3.46E+17 | 1.89E+19 | 5.22E+15 | 1.09E+18 |
| 57.30 | 1.31E+20 | 2.43E+16 | 3.80E+17 | 2.17E+19 | 6.38E+15 | 1.44E+18 |
| 62.08 | 1.41E+20 | 2.84E+16 | 4.14E+17 | 2.46E+19 | 7.66E+15 | 1.85E+18 |
| 66.85 | 1.50E+20 | 3.28E+16 | 4.48E+17 | 2.76E+19 | 9.05E+15 | 2.33E+18 |
| 71.63 | 1.59E+20 | 3.75E+16 | 4.83E+17 | 3.07E+19 | 1.05E+16 | 2.88E+18 |
| 76.40 | 1.68E+20 | 4.25E+16 | 5.18E+17 | 3.39E+19 | 1.22E+16 | 3.51E+18 |
| 81.18 | 1.77E+20 | 4.79E+16 | 5.54E+17 | 3.72E+19 | 1.39E+16 | 4.21E+18 |
| 85.95 | 1.86E+20 | 5.36E+16 | 5.90E+17 | 4.05E+19 | 1.57E+16 | 4.99E+18 |
| 90.73 | 1.94E+20 | 5.96E+16 | 6.27E+17 | 4.40E+19 | 1.76E+16 | 5.84E+18 |
| 95.50 | 2.02E+20 | 6.60E+16 | 6.65E+17 | 4.75E+19 | 1.96E+16 | 6.78E+18 |
| 100.28 | 2.11E+20 | 7.28E+16 | 7.03E+17 | 5.11E+19 | 2.17E+16 | 7.80E+18 |
| 105.05 | 2.19E+20 | 8.00E+16 | 7.42E+17 | 5.48E+19 | 2.39E+16 | 8.90E+18 |
| 109.83 | 2.27E+20 | 8.75E+16 | 7.81E+17 | 5.86E+19 | 2.61E+16 | 1.01E+19 |
| 114.60 | 2.34E+20 | 9.54E+16 | 8.22E+17 | 6.25E+19 | 2.85E+16 | 1.13E+19 |
| 119.38 | 2.42E+20 | 1.04E+17 | 8.63E+17 | 6.64E+19 | 3.09E+16 | 1.27E+19 |
| 124.15 | 2.49E+20 | 1.12E+17 | 9.04E+17 | 7.04E+19 | 3.34E+16 | 1.41E+19 |
| 128.93 | 2.56E+20 | 1.21E+17 | 9.47E+17 | 7.46E+19 | 3.60E+16 | 1.56E+19 |
| 133.70 | 2.63E+20 | 1.31E+17 | 9.91E+17 | 7.88E+19 | 3.87E+16 | 1.72E+19 |
| 138.48 | 2.70E+20 | 1.41E+17 | 1.03E+18 | 8.31E+19 | 4.14E+16 | 1.88E+19 |
| 143.25 | 2.77E+20 | 1.51E+17 | 1.08E+18 | 8.75E+19 | 4.42E+16 | 2.05E+19 |
| 148.03 | 2.84E+20 | 1.62E+17 | 1.13E+18 | 9.20E+19 | 4.71E+16 | 2.23E+19 |
| 152.80 | 2.90E+20 | 1.73E+17 | 1.17E+18 | 9.66E+19 | 5.01E+16 | 2.42E+19 |
| 157.58 | 2.96E+20 | 1.85E+17 | 1.22E+18 | 1.01E+20 | 5.31E+16 | 2.62E+19 |
| 162.35 | 3.02E+20 | 1.97E+17 | 1.27E+18 | 1.06E+20 | 5.62E+16 | 2.82E+19 |
| 167.13 | 3.08E+20 | 2.10E+17 | 1.32E+18 | 1.11E+20 | 5.94E+16 | 3.03E+19 |
| 171.90 | 3.14E+20 | 2.23E+17 | 1.37E+18 | 1.16E+20 | 6.27E+16 | 3.24E+19 |
| 176.68 | 3.19E+20 | 2.36E+17 | 1.42E+18 | 1.21E+20 | 6.61E+16 | 3.47E+19 |
| 181.45 | 3.24E+20 | 2.50E+17 | 1.48E+18 | 1.26E+20 | 6.95E+16 | 3.70E+19 |
| 186.23 | 3.30E+20 | 2.65E+17 | 1.53E+18 | 1.31E+20 | 7.30E+16 | 3.94E+19 |
| 191.00 | 3.34E+20 | 2.80E+17 | 1.59E+18 | 1.37E+20 | 7.66E+16 | 4.18E+19 |

For comparison to the MHR maximum burnup compact, a maximum burnup, or maximum % FIMA compact was chosen from the AGR-1 test capsules. The particular compact chosen was from capsule 4, stack1 (facing the core) with a calculated 19.8 % FIMA (187.42 GWD/MTU). Overall, the % FIMA for the AGR-1 compacts ranged from 11.4-19.8%.[9]

## AGR-1 Mass Isotopics

Figures 9 and 10 are identical plots of the specific isotopic mass (g/g uranium initial), except Figure 9 is plotted as a function of ATR cycle and Figure 10 is plotted as a function of burnup (GWD/MTU). In Figure 10, it is interesting to note that the maximum burnup achieved by this high-burnup AGR-1 fuel compact at the end of cycle 145A was approximately 187 GWD/MTU. This is approximately equal to the assumed maximum burnup of the MHR fuel at approximately 191 GWD/MTU.

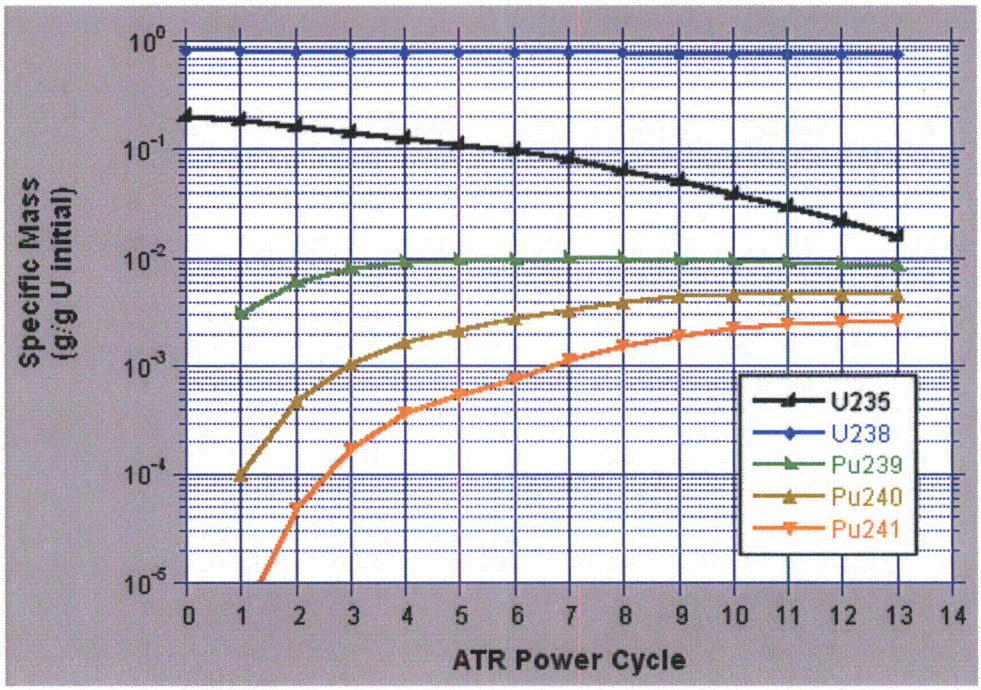


Figure 9. AGR-1 fuel isotopic specific MASS as a function of ATR power cycle.

9. INL ECAR-958 (2010) Sterbentz, J. W., "JMOCUP As-Run Daily Depletion Calculation for the AGR-1 Experiment in the ATR B-10 Position," Idaho National Laboratory Engineering Calculations and Analysis Report 958 (ECAR-958), Revision 0, May 2010.

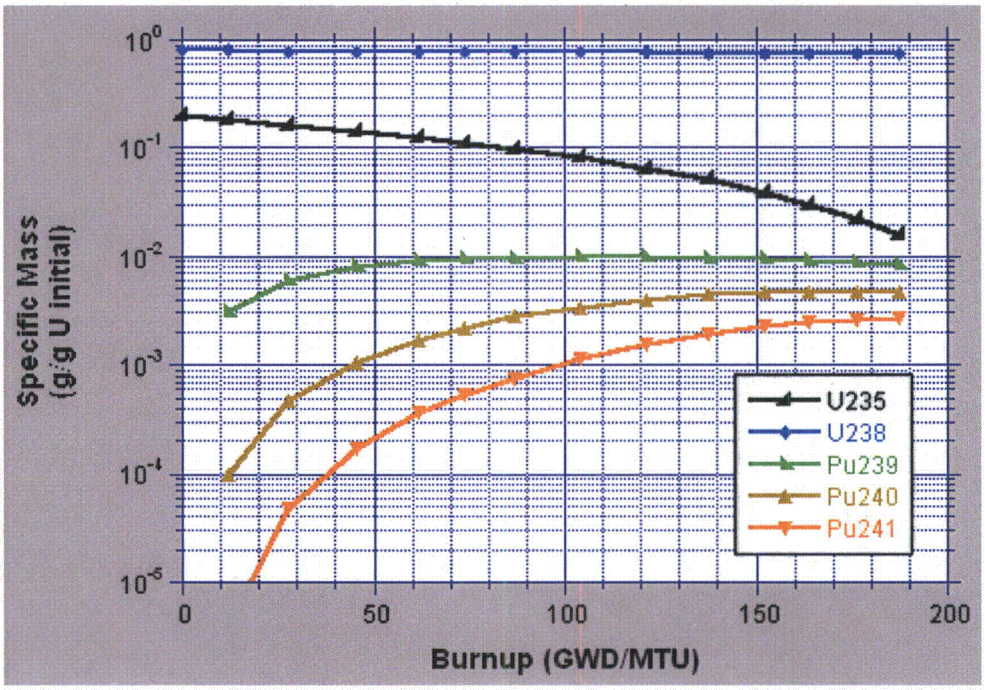


Figure 10. AGR-1 fuel isotopic specific MASS as a function of burnup (GWD/MTU).

The AGR-1 maximum burnup compact contained approximately 4,370 TRISO particles; 92.05% of the U-235 atoms or mass was depleted during the 13 ATR cycles with approximately 17-18% transmuting into U-236 and the rest fissioning; 7.8% of the U-238 was depleted with approximately 99% transmuting into Pu-239. In addition, the compact power ranged from 220–460 watts or 50–105 milliwatts per particle over the course of the 13 ATR power cycles.

## AGR-1 Fissions

Figure 11 shows the AGR-1 isotopic fissions as a function of burnup for the maximum burnup AGR-1 TRISO-particle fuel compact. The fissions have been divided by the beginning-of-life mass of uranium (U-235 and U-238) in order to make a one-to-one comparison with the MHR fuel burnup analysis (Figure 7 and Table 1). The wiggle in the Figure 11 curves is due to both the statistical nature of the MCNP5-calculated fission cross sections and the variation in the ATR cycle power and length.

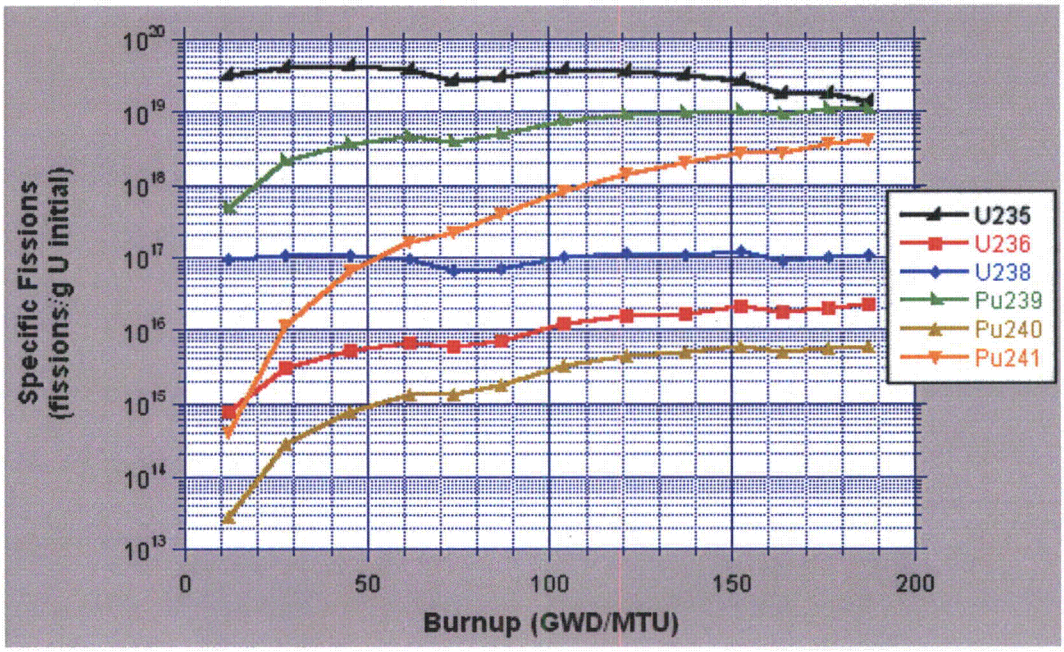


Figure 11. AGR-1 fuel isotopic specific FISSIONS as a function of burnup.

Note that by the end of the last ATR power cycle (145A), the number of U-235 and Pu-239 fissions is comparable.

Table 3 gives the calculated data plotted in Figure 11, or the specific isotopic fissions per ATR cycle for U-235, U-236, U-238, Pu-239, Pu-240, and Pu-241. At the bottom of the table are the isotopic fission totals. Total fissions by cycle are given in the right column.

Table 3. AGR-1 isotopic fissions (fissions/g U initial) as a function of ATR cycle and burnup.

| ATR Cycle | Burnup (GWD/MTU) | U-235 | U-236 | U-238 | Pu-239 | Pu-240 | Pu-241 | TOTAL |
|---|---|---|---|---|---|---|---|---|
| 138B | 11.92 | 3.15E+19 | 7.86E+14 | 9.52E+16 | 4.85E+17 | 2.83E+13 | 3.93E+14 | 3.21E+19 |
| 139A | 27.84 | 4.06E+19 | 3.00E+15 | 1.09E+17 | 2.08E+18 | 2.74E+14 | 1.13E+16 | 4.28E+19 |
| 139B | 45.38 | 4.32E+19 | 5.16E+15 | 1.05E+17 | 3.71E+18 | 7.67E+14 | 6.36E+16 | 4.71E+19 |
| 140A | 61.83 | 3.92E+19 | 6.54E+15 | 9.45E+16 | 4.65E+18 | 1.31E+15 | 1.64E+17 | 4.41E+19 |
| 140B | 73.62 | 2.73E+19 | 5.75E+15 | 6.61E+16 | 3.98E+18 | 1.30E+15 | 2.22E+17 | 3.16E+19 |
| 141A | 86.90 | 3.01E+19 | 7.23E+15 | 7.11E+16 | 5.00E+18 | 1.78E+15 | 3.94E+17 | 3.55E+19 |
| 142A | 104.05 | 3.74E+19 | 1.20E+16 | 1.01E+17 | 7.47E+18 | 3.21E+15 | 8.35E+17 | 4.58E+19 |
| 142B | 121.28 | 3.56E+19 | 1.53E+16 | 1.12E+17 | 8.87E+18 | 4.37E+15 | 1.39E+18 | 4.60E+19 |
| 143A | 137.46 | 3.13E+19 | 1.68E+16 | 1.06E+17 | 9.66E+18 | 4.79E+15 | 1.99E+18 | 4.31E+19 |
| 143B | 152.53 | 2.66E+19 | 2.06E+16 | 1.19E+17 | 1.05E+19 | 5.96E+15 | 2.66E+18 | 4.00E+19 |
| 144A | 163.84 | 1.81E+19 | 1.70E+16 | 9.00E+16 | 9.00E+18 | 4.81E+15 | 2.66E+18 | 2.99E+19 |
| 144B | 176.40 | 1.81E+19 | 1.99E+16 | 9.90E+16 | 1.12E+19 | 5.50E+15 | 3.74E+18 | 3.31E+19 |
| 145A | 187.42 | 1.36E+19 | 2.27E+16 | 1.08E+17 | 1.12E+19 | 6.03E+15 | 4.05E+18 | 2.89E+19 |
| | TOTAL | 3.93E+20 | 1.53E+17 | 1.28E+18 | 8.78E+19 | 4.01E+16 | 1.82E+19 | 5.00E+20 |

The Table 3 data—which are the fissions accumulated by the end of each cycle—are based on detailed fission isotopic reaction rates at each timestep during the respective ATR power cycle. For the 13 ATR power cycles comprising the AGR-1 test, there were a total of 662 timesteps. The AGR-1 JMOCUP depletion calculation was a very detailed, high-resolution depletion analysis.

A comparison of Table 1 (MHR) and Table 3 (AGR-1) total specific isotopic fissions (fissions/g uranium initial) data shows the AGR-1 maximum burnup compact experienced 1.18 times more U-235 fissions (3.93E + 20) than the MHR fuel (3.34E + 20). On the other hand, the MHR total Pu-239 fissions were higher by a factor of 1.56 (1.37E+20 versus 8.78E+19 fissions/g U initial). Similarly, the MHR Pu-240 and Pu-241total fissions were higher than the AGR-1 test by factors of 1.91 and 2.30, respectively. The total fissions for both the MHR and AGR-1 were comparable at 5.15E+20 and 5.00E+20, respectively, with the MHR having slightly more total fissions.

Figure 12 shows the AGR-1 cumulative isotopic fissions per initial mass of uranium as a function of burnup.

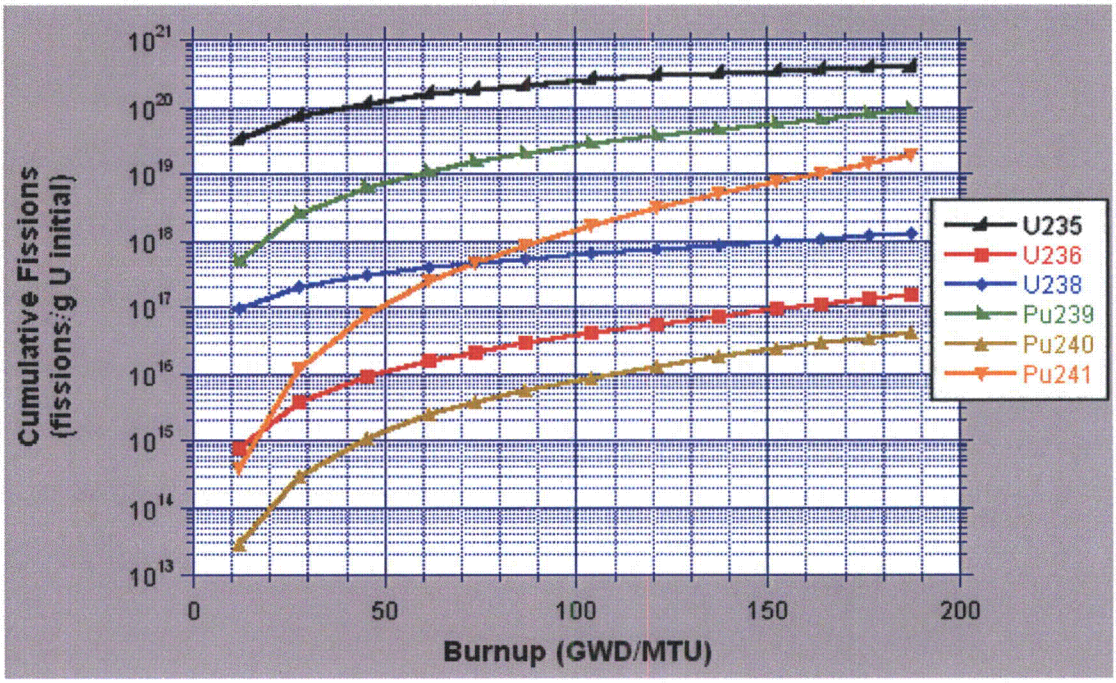


Figure 12. AGR-1 cumulative specific FISSIONS as a function of burnup (GWD/MTU).

Table 4 gives the AGR-1 cumulative specific isotopic fissions for U-235, U-236, U-238, Pu-239, Pu-240, and Pu-241 fissions by ATR cycle. These are the same data plotted in Figure 12, plus at the bottom of the table are the isotopic totals and cumulative total by cycle in the far right column.

Table 4. Cumulative AGR-1 isotopic fissions (fissions/g U initial) by ATR cycle and burnup.

| ATR Cycle | Burnup (GWD/MTU) | U-235 | U-236 | U-238 | Pu-239 | Pu-240 | Pu-241 | TOTAL |
|---|---|---|---|---|---|---|---|---|
| 138B | 11.92 | 3.15E+19 | 7.86E+14 | 9.52E+16 | 4.85E+17 | 2.83E+13 | 3.93E+14 | 3.21E+19 |
| 139A | 27.84 | 7.22E+19 | 3.78E+15 | 2.04E+17 | 2.57E+18 | 3.02E+14 | 1.17E+16 | 7.49E+19 |
| 139B | 45.38 | 1.15E+20 | 8.94E+15 | 3.09E+17 | 6.28E+18 | 1.07E+15 | 7.53E+16 | 1.22E+20 |
| 140A | 61.83 | 1.55E+20 | 1.55E+16 | 4.03E+17 | 1.09E+19 | 2.38E+15 | 2.40E+17 | 1.66E+20 |
| 140B | 73.62 | 1.82E+20 | 2.12E+16 | 4.69E+17 | 1.49E+19 | 3.68E+15 | 4.61E+17 | 1.98E+20 |
| 141A | 86.90 | 2.12E+20 | 2.84E+16 | 5.40E+17 | 1.99E+19 | 5.46E+15 | 8.55E+17 | 2.33E+20 |
| 142A | 104.05 | 2.49E+20 | 4.04E+16 | 6.42E+17 | 2.74E+19 | 8.67E+15 | 1.69E+18 | 2.79E+20 |
| 142B | 121.28 | 2.85E+20 | 5.58E+16 | 7.54E+17 | 3.63E+19 | 1.30E+16 | 3.08E+18 | 3.25E+20 |
| 143A | 137.46 | 3.16E+20 | 7.26E+16 | 8.59E+17 | 4.59E+19 | 1.78E+16 | 5.07E+18 | 3.68E+20 |
| 143B | 152.53 | 3.43E+20 | 9.31E+16 | 9.78E+17 | 5.64E+19 | 2.38E+16 | 7.74E+18 | 4.08E+20 |
| 144A | 163.84 | 3.61E+20 | 1.10E+17 | 1.07E+18 | 6.54E+19 | 2.86E+16 | 1.04E+19 | 4.38E+20 |
| 144B | 176.40 | 3.79E+20 | 1.30E+17 | 1.17E+18 | 7.66E+19 | 3.41E+16 | 1.41E+19 | 4.71E+20 |
| 145A | 187.42 | 3.93E+20 | 1.53E+17 | 1.28E+18 | 8.78E+19 | 4.01E+16 | 1.82E+19 | 5.00E+20 |

### 2.2.4 Summary Comparison of the AGR-1 and the prismatic MHR TRISO Fuel Burnup Characteristics

A comparative burnup study was performed to support and quantitatively estimate potential differences in palladium and silver fission product concentrations in TRISO fuel compacts irradiated in the AGR-1 test and in a hypothetical NGNP prismatic high temperature gas reactor which we have assumed here to be the General Atomics modular helium reactor (MHR). The study compared maximum burnup compacts containing TRISO fissile-particles; the AGR-1 compact had a burnup of 19.8 % FIMA (187 GWD/MTU) and the MHR compact 19.9 % FIMA (191 GWD/MTU). The goal was to compare these two maximum burnup compacts, and see if the resulting AGR-1 compacts produced more or less palladium and silver than the MHR maximum burnup compacts.

Only fissile-particles were considered in the study, primarily because the AGR-1 test used only single fissile-particles with an enrichment of 19.9 wt% U-235. Fortunately, the recent General Atomics core performance design study[8] also used a fissile-particle with a 19.9 wt% U-235 enrichment and published the maximum expected fissile-particle burnup (19.7–20.2 % FIMA). A reasonable one-to-one burnup comparison could then be performed.

The prismatic burnup study first considered the neutron spectral differences in both the AGR-1 test (ATR) and the MHR. The thermal neutron flux magnitude in the AGR-1 test increased with each ATR power cycle due to burnable poison depletion, but the thermal flux peak remained fixed at approximately 0.09 eV. The thermal neutron flux peak in the MHR was higher in energy (0.3 eV) indicating a harder spectrum and overlaying the Pu-239 fission and capture resonance channels at 0.3 eV with the expected result of relatively higher Pu-239 fission rates, higher Pu-240 and Pu-241 production rates, and higher Pu-241 fission rates, and this is born out in the calculated results of the burnup analysis here.

The burnup study focused on the primary isotopic actinides which include U-235, U-236, U-238, Pu-239, Pu-240, and Pu-241. Other actinides are obviously produced, but in relatively smaller quantities and are not considered in the discussion. Considering only these six actinides, the MHR maximum burnup compact produced slightly more total specific fissions than the maximum burnup MHR compacts, or 5.15E+20 versus 5.00E+20 fissions/g U initial. The AGR-1 fuel experienced 1.18 times more U-235 fissions (3.93E + 20) than the MHR fuel (3.34E + 20). However, the MHR total Pu-239 fissions were higher by a factor of 1.56, or 1.37E+20 versus 8.78E+19 fissions/g U initial. Similarly, the MHR Pu-240 and Pu-241total fissions were higher than the AGR-1 test by factors of 1.91 and 2.30, respectively. The higher plutonium fissions was expected based on the

neutron spectral differences, since the MHR and AGR-1 maximum burnups were nearly equal (191 versus 187 GWD/MTU).

Figure 13 shows the difference in the cumulative fissions of U-235 and Pu-239 for the AGR-1 and MHR cases. AGR-1 accumulated more U-235 fissions as previously mentioned, whereas the MHR accumulated more Pu-239 fissions.

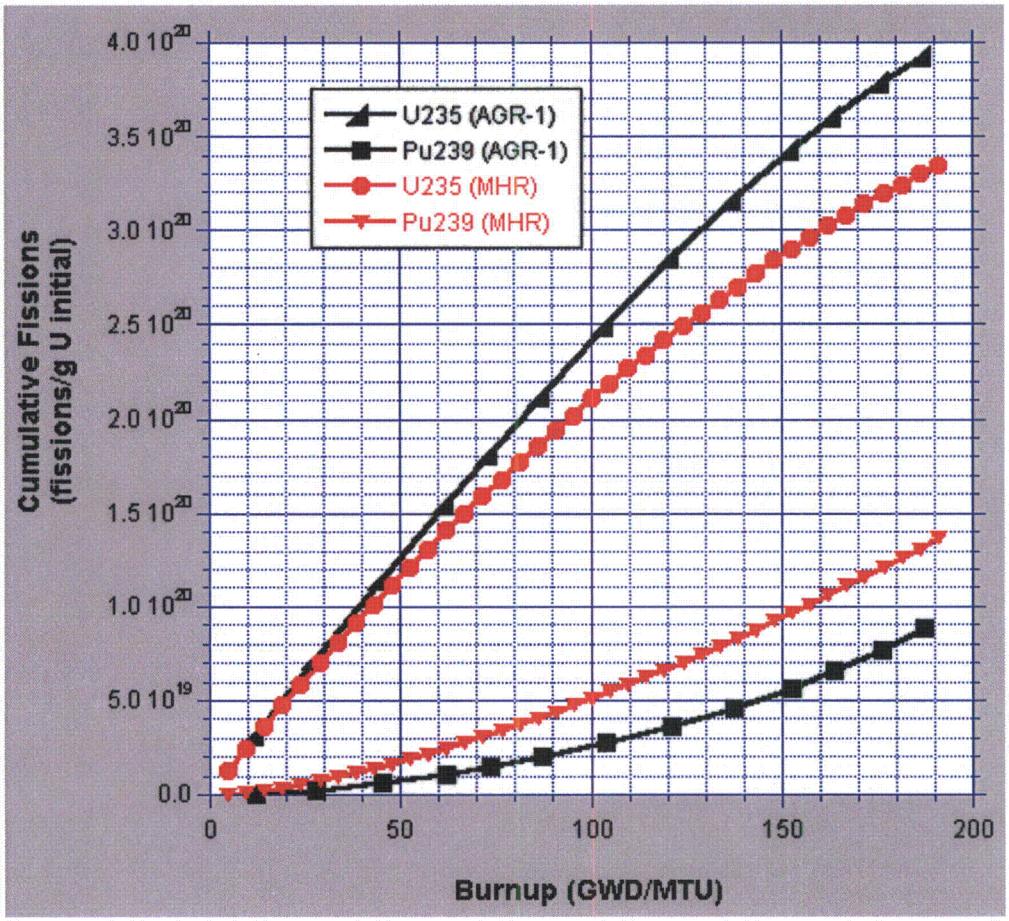


Figure 13. AGR-1 and MHR comparison of the cumulative specific fissions for Pu-239, Pu-241, and U-235 as a function of burnup (GWD/MTU).

Table 5 gives the isotopic fission percentage for the AGR-1 and MHR cases. It is clear that U-235 is by far the largest contributor to the total number of fissions followed by Pu-239 and Pu-241. The fertile actinides U-236, U-238, and Pu-240 are minor contributors to the total number of fissions.

Table 5. Percentage of the total specific fissions (fissions/g U initial) by isotope for the AGR-1 test and the MHR.

| Case | U-235 | U-236 | U-238 | Pu-239 | Pu-240 | Pu-241 |
|---|---|---|---|---|---|---|
| AGR-1 | 78.6% | 0.03% | 0.26% | 17.6% | 0.008% | 3.64% |
| MHR | 64.9% | 0.05% | 0.31% | 26.6% | 0.015% | 8.11% |

The higher number of MHR plutonium fissions relative to AGR-1 raises a question as to how much more palladium and silver is produced in the MHR compacts versus those in the AGR-1 test, because palladium fission product yields for thermal fission of Pu-239 and Pu-241 are 8.9 and 13.0 times higher than for the thermal fission of U-235. Likewise, silver (Ag-109) fission product yields for thermal fission of Pu-239 and Pu-241 are 32.0 and 53.0 times higher than for a U-235 thermal fission. The palladium and silver production in the maximum burnup MHR and AGR-1 compacts is compared next.

First the palladium and silver isotopes and their corresponding beta-decay chains are identified. Fission product beta-decay chains producing palladium atoms include the A=105, 106, 107, 108, and 110 chains. For silver, it is just the A=109 chain. Table 6 gives total fission product yield (%) for each decay chain ending in the end product isotope (Pd-105, Pd-106, Pd-107, Pd-108, Pd-110, and Ag-109). These yields are for thermal fission of U-235, Pu-239, and Pu-241, and fast fission for U-238. These yield estimates are from the high temperature gas-cooled reactor cross section library from the ORIGEN2.2 computer code (no data were available for U-236 or Pu-240).

Table 6. Isotopic fission product yields (%) for palladium and silver isotopes.

| Fission Product | U-235 | U-238 | Pu-239 | Pu-241 |
|---|---|---|---|---|
| Pd-105 | 1.039 | 3.854 | 5.369 | 6.150 |
| Pd-106 | 0.415 | 2.573 | 4.312 | 6.188 |
| Pd-107 | 0.193 | 1.477 | 3.216 | 5.293 |
| Pd-108 | 0.0915 | 0.953 | 2.234 | 4.036 |
| Pd-110 | 0.0326 | 0.610 | 0.627 | 1.231 |
| Ag-109 | 0.0446 | 0.770 | 1.440 | 2.362 |

Table 6 data was used along with isotopic specific fissions from Table 1 (MHR) and Table 3 (AGR-1) data to estimate the production of palladium and silver atoms per g U initial as a function of burnup for the AGR-1 and MHR cases. For the palladium and silver contributions from U-236 and Pu-240, the calculation simply used the U-238 yields, although the U-238, U-236, Pu-240 contributions were relatively minor compared to U-235, Pu-239, and Pu-241.

The total cumulative number of palladium atoms generated at the end of burnup for the maximum burnup MHR fuel was estimated to be 3.74E+19 atoms Pd/g U initial, and for the maximum burnup AGR-1 fuel 2.51E+19 atoms Pd/g U initial. The MHR case therefore has an estimated 49.1% higher concentration of palladium fission product atoms relative to the AGR-1 maximum burnup compact.

Similarly for Ag-109, the total cumulative number of silver atoms generated at the end of burnup for the maximum burnup MHR fuel was estimated to be 3.12E+18 atoms Ag/g U initial; and for the maximum burnup AGR-1 fuel 1.88E+18 atoms Ag/g U initial. The MHR case has an estimated 66.0% higher concentration of silver fission product atoms relative to the AGR-1 maximum burnup compact.

From the AGR-1 and MHR burnup analysis, it is clear that the MHR maximum burnup fissile-particles will produce higher quantities of palladium and silver in maximum burnup fissile-particles. The estimated relative magnitudes of palladium and silver are higher by factors of 1.49 and 1.66, respectively. These differences are significant, butdespite the order of magnitude differences in the fission product yields of palladium and silver from plutonium fission and the higher MHR plutonium fission fraction, the palladium and silver atom concentrations are not orders of magnitudes larger relative to the AGR-1 test. The main reason is that the bulk of both the AGR-1 and MHR fissions are from U-235, 78.6% and 64.9%, respectively, and not plutonium.

Furthermore, one can expect smaller palladium and silver concentration differences between AGR-1and MHR fuel for lower burnups. This conclusion is based on the smaller differences between the AGR-1 and MHR Pu-239 curves in Figure 13.

### 2.2.5 Pebble Bed HTGR Burnup Characteristics

Some of the burnup characteristics of pebble bed fuel were computed and are described here. A Pebble Bed Reactor (PBR) with recirculating fuel is difficult to model with MCNP and ORIGEN so the PEBBED[10] code was used. Developed at Idaho National Laboratory (INL), PEBBED performs a coupled neutronic-thermal fluid analysis of the core with a burnup simulation that converges directly upon the equilibrium or asymptotic state of the core. Pebble flow is assumed to be purely axial (i.e., a flat core bottom) but the isotopic error induced by neglecting the bottom discharge conus is considered to be minor. PEBBED performs online cross-section generation using COMBINE7.1. The core and reflector regions are divided into 'spectral zones' in each of which the spectrum and microscopic cross sections are assumed to be uniform. The 1-D transport solver in COMBINE is

10. Gougar, H. D., et al. (2010) "Automated Design and Optimization of Pebble Bed Reactor Cores," Nuclear Science and Engineering, Volume 165, No. 3, July 2010.

used in a multistage fashion in the pebble bed itself, sequentially solving the transport equation and homogenizing the cross sections over the particle and pebble. A 1-D radial model of the core from centerline out through the core barrel is then executed with the homogenized cross-sections from the pebble region solution comprising the source term. No PBR has ever operated in its asymptotic burnup state so this equilibrium cycle calculation cannot be validated. PEBBED results do, however, compare favorably to equilibrium core benchmark calculations performed using VSOP and WIMS.[11]

The reference core in this case is the PBMR400, a 400 MWth pebble bed reactor with a 500°C inlet temperature and a 900°C outlet temperature. A detailed description of this design is given in by Reitsma.[12] A pebble contains 9 grams of UO2 enriched to 9.6%. Each is dropped into, and passes through, the core six times before final discharge at approximately 96 GWD/MTU, or 10.4% FIMA.

The Pebble Bed Modular Reactor (PBMR)400 uses neither burnable poisons nor fuel zoning to flatten the power profile. Stress on the fuel is limited by the fact that a given pebble never remains in a 'hotspot' for very long. The pebble bed itself provides a more coolable configuration than a comparable prismatic core so the average fuel temperature is somewhat lower. Online refueling eliminates the need for significant excess reactivity, hence the comparably lower feed enrichment.

The flux and temperature variability within the core combined with the stochastic loading pattern results in considerable variation in the spectrum to which the pebbles are exposed. Figures 13 and 14 are profiles (fast and thermal flux, respectively) in the PBMR400. The aspect ratio (height to width) has been deliberately lowered for the purposes of illustration. The thin white rectangle indicates the boundaries of the core itself.

The fast flux peaks in the radial center of the core annulus but is closer to the top of the core because of the lower temperature and average burnup in that region. The thermal flux peaks just outside the core in the inner reflector. Part of the flux variation results from the temperature gradient. The coolant increases in temperature by about 500°C from the top to the bottom of the core as shown in Figure 15. This is higher than the plenum-to-plenum core temperature rise (400°C) because, in this model, about 18% of the coolant bypasses the core, flows through the outer reflector, and mixes with the core outlet stream to yield a lower average for the mixture.

---

11. B. Tyobeka and F. Reitsma, Results of the IAEA CRP5 – Benchmark Analysis Related to the PBMR-400, PBMM, GT-MHR, HTR-10 and the ASTRA Critical Facility, Proceedings of PHYSOR 2010 – Advances in Reactor Physics to Power the Nuclear Renaissance, Pittsburgh, PA, May 9-14, 2010.

12 Reitsma, F. (2004) "The Pebble Bed Modular Reactor Layout and Neutronics Design of the Equilibrium Cycle," Proceedings of PHYSOR2004 Conference, Chicago, USA, April 25-29, 2004.

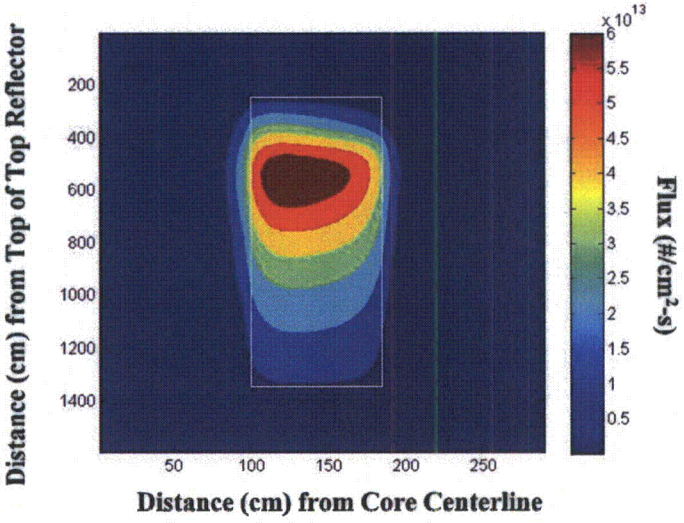


Figure 13. Fast (>1.86 eV) Flux Profile in the PBMR 400.

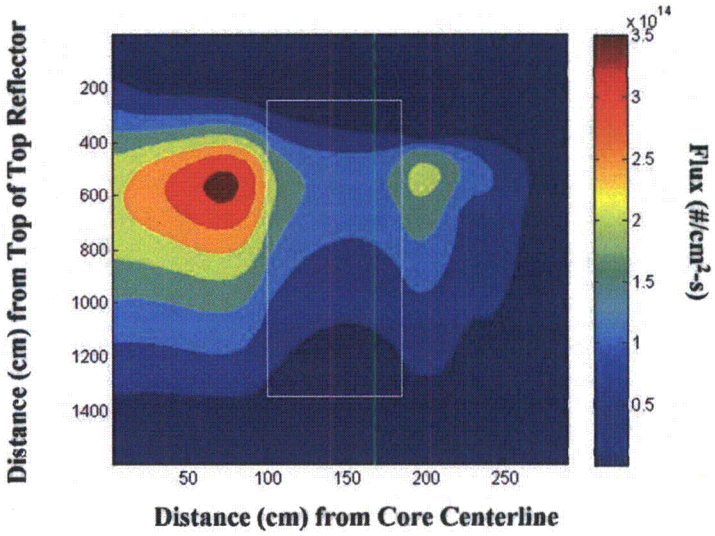


Figure 14. Thermal (<1.86 eV) Flux Profile in the PBMR 400.

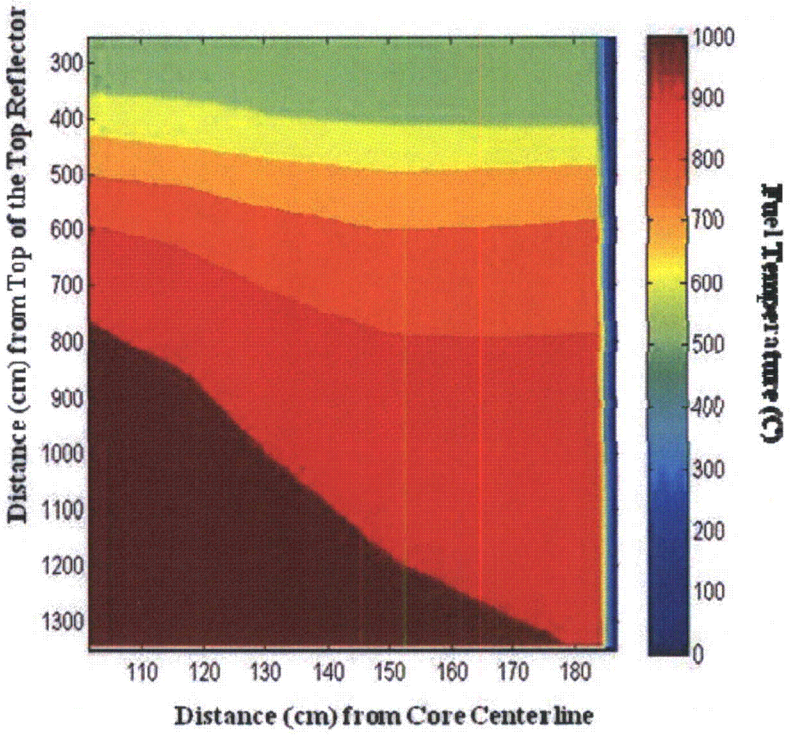


Figure 15. Temperature Profile in the PBMR 400.

Clearly, the spectrum will be a strong function of position in this core. To confirm this, the spectra were computed for selected regions of the core (orange rectangles in Figure 16). The locations of the regions correspond to either the upper (U), midplane (M), or lower (L) part of the core annulus and either near the inner reflector (edge) or the middle of the core annulus (mid). The spectrum for each of these regions was extracted from the converged PEBBED-COMBINE solution and plotted in Figures 17 and 18.

The left plot of Figure 17 shows how the spectrum varies near the inner reflector in going from the top to the bottom. Like the prismatic MHR, the thermal flux peak occurs at about 0.3 eV thus the overall spectra of these two reactor concepts are comparable. There is little difference between the middle and lower regions of the core but a significant difference between the lower and upper regions. Even though the temperature is higher at the bottom, the higher burnup and effect of the bottom reflector make for a softer spectrum in the bottom part of the core. The fuel temperatures in these regions are roughly 550 °C (upper), 980 °C, (midplane), and 1010 °C (lower). The plot at the right in Figure 17 shows the difference in the spectra between the edge and the radial middle of the core annulus. The spectrum is significantly harder in the middle as could be inferred from Figures 13 and 14.

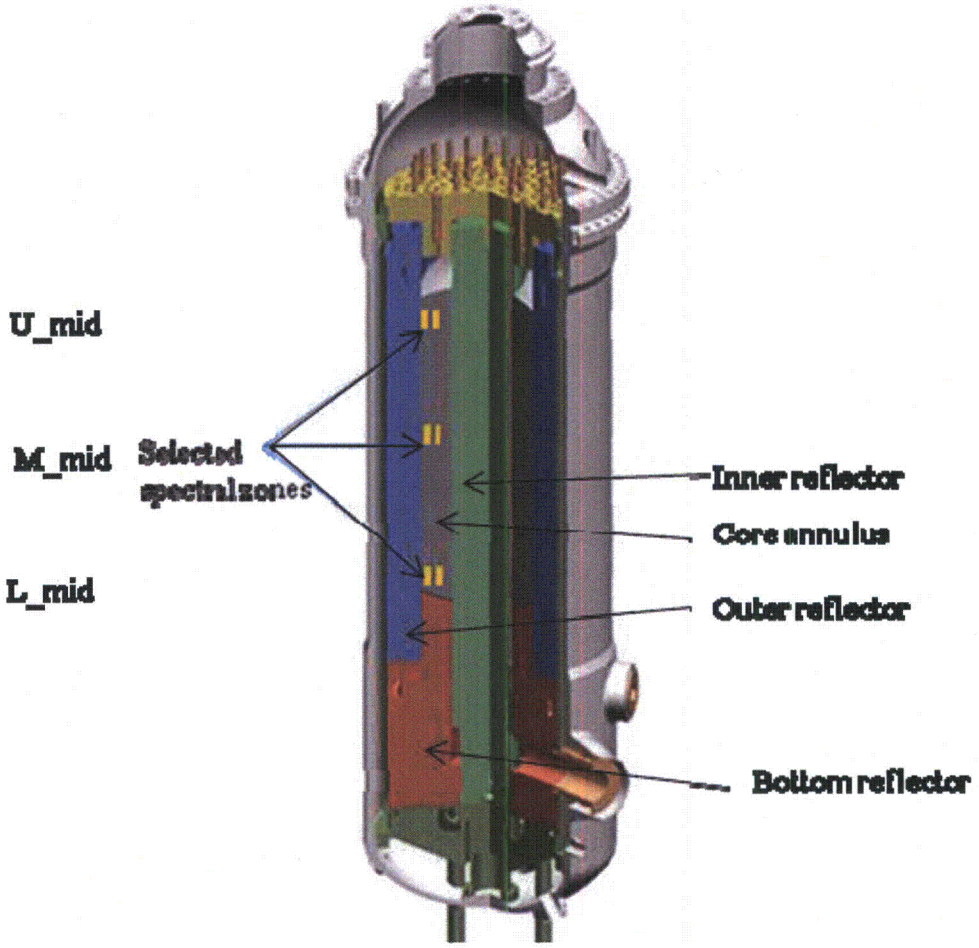


Figure 16. PBMR 400 showing selected spectral zones.

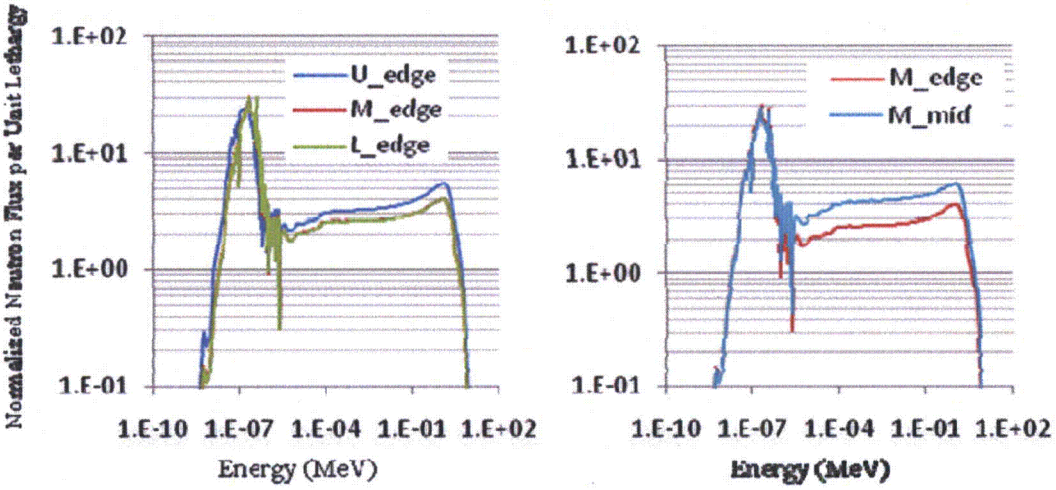


Figure 17. Spectra at three point near the inner reflector (left) and at two points near the core midplane (right).

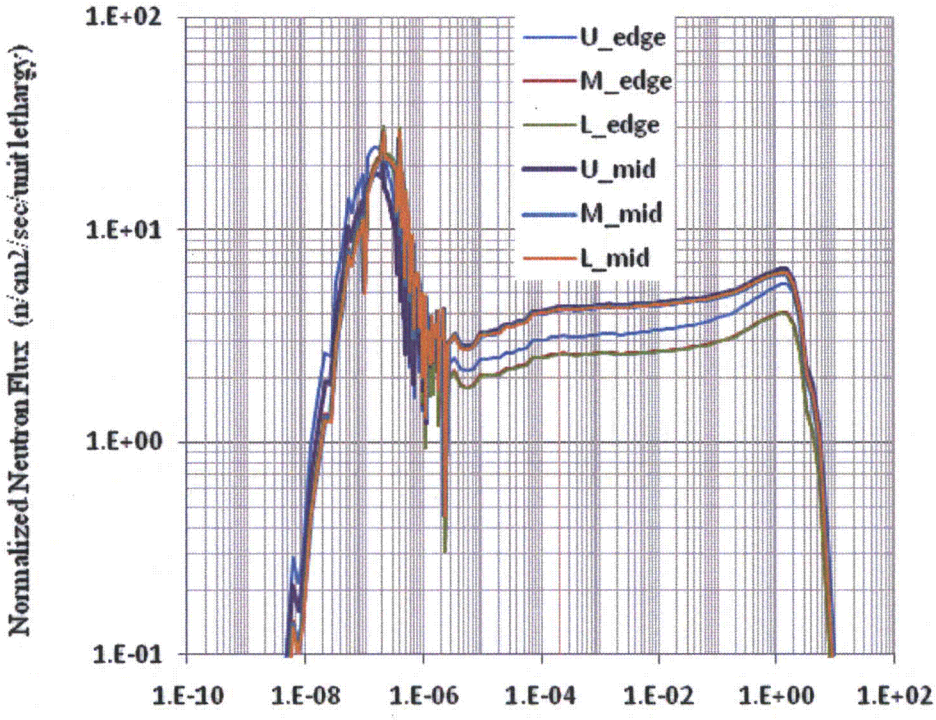


Figure 18. Spectra at all 6 Selected Regions of the PBMR core.

In both plots, a particular difference is observed in the low resonance region around 1 eV. As this is the location of a pronounced capture peak in Pu-240, one would expect considerable variability in the concentration of higher plutonium and minor actinides in spent pebbles.

In Figure 18, all 6 of the spectra were plotted to illustrate the spectral envelope in which pebbles are burned.

A comparison of the spectral shape in Figure 18 with those in Figure 4 reveals that the PBMR400 spectrum is very similar to that of the prismatic MHR. Close examination reveals that the PBMR400 thermal flux peak peaks near 0.2 eV while the prismatic peak is a bit closer to 0.3 eV; both being much higher than the AGR thermal flux peak (~0.1 eV). The PBMR400 core has a moderating ratio (atoms of carbon to atoms of uranium) of around 430 (reflector carbon neglected) which is higher than that of the prismatic core value of 360. This higher value leads to slightly better thermalization.

The evolution of the fission source is plotted in Figure 19. This plot exhibits the same trends as the prismatic HTGR data shown in Figure 11. The U-235 and Pu-239 values are in good agreement with the prismatic HTGR values. The curves for the remaining fissionable isotopes show less agreement but they also represent only a small fraction of the total fissions. At 10.4% FIMA (~97 GWD/MTU) (the discharge burnup of PBMR400 fuel), the ratio of specific fissions of Pu-239 to the total is about 32% in the PBMR400 fuel compared to 27% for the prismatic fuel. This can be attributed to the slightly softer spectrum which would yield a lower production-to-fission ratio in that isotope.

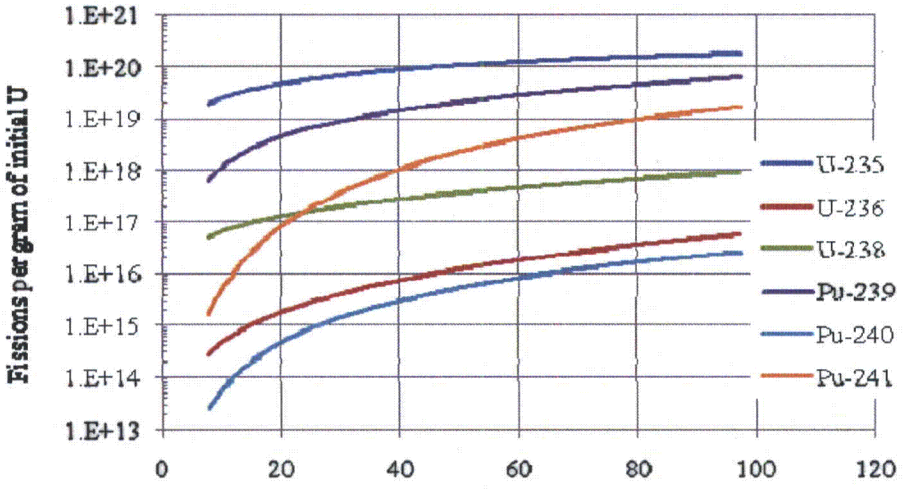


Figure 19. Cumulative Specific Fissions as a Function of Burnup.

At the discharge burnup of PBMR400 fuel (~ 97 GWD/MTU), the cumulative specific fissions (fissions/initial gram of uranium) of Pu-239 are listed here.

| | |
|---|---|
| AGR-1: | 2.5E19 |
| MHR | 5.1E19 |
| PBMR400 | 6.3E19 |

Both the prismatic and pebble bed HTGR values are, however, bounded by the total specific fissions attained in the AGR-1 test, 8.8E19, with some margin to allow for the variances that result from the nonuniform flux profiles. Even with computed variation in the burnup of pebbles discharged from the PBMR400 (shown in Figure 20), the total number of plutonium fissions is still bounded by the AGR-1 test at final burnup. The peak burnup is about 6% higher than the expected value so the corresponding peak cumulative specific fission value is about 6.7E19 and still less than the prismatic HTGR. The variability in burnup is somewhat less than that expected in a comparable prismatic reactor because the pebbles are randomly loaded and moving through the core. Except for a

statistically negligible number, all of the pebbles are subjected to the radial and axial variation in the core.

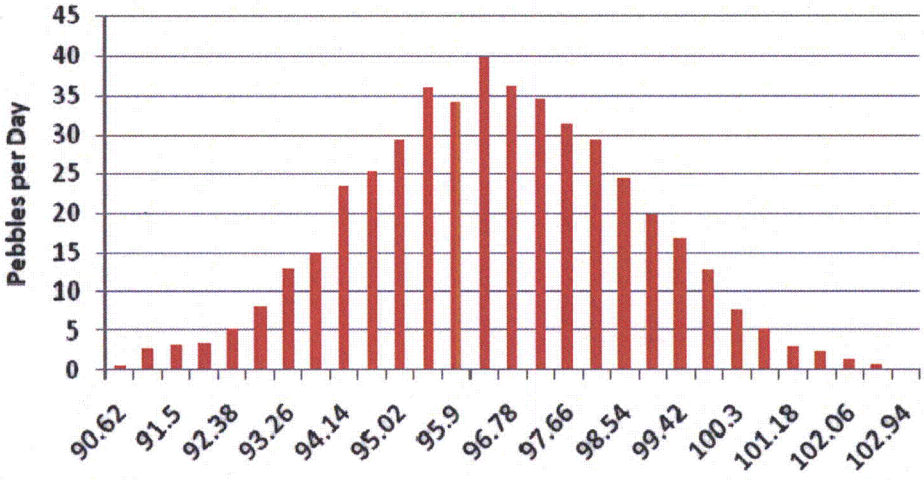


Figure 20. Discharge Burnup Variability in the PBMR400 (GWD/MTU).

The effect on discharge isotopics of the spectral variability in the core is illustrated in Figures 21 through 26. In each, the specific mass in discharged pebbles of a particular isotope or group of isotopes of interest is plotted as a histogram. At full power equilibrium, the PBMR400 consumes about 466 fresh pebbles per day and discharges the same amount of spent pebbles.

Figure 21 shows the specific mass (discharged mass per mass of uranium in fresh fuel) of all plutonium in spent pebbles. The variability is significant; the difference between the minimum and maximum of values is about 27% of the mean.

The shape is decidedly not Gaussian (symmetric bell curve) and is almost entirely due to the Pu-239 contribution shown in Figure 22. The source of Pu-239 (from U-238 capture) is largely constant over the life of the pebble owing to the large fraction of U-238 in the fuel. The destruction of Pu-239, however, is more sensitive to the local spectrum and this leads to the irregular distribution of Pu-239 in discharged fuel.

The average Pu-239 buildup in the pebble is about 4.5 mg/g initial U, somewhat less than half that of the MHR because of the softer spectrum. The plot indicates, however, that the spread between the minimum and maximum Pu-239 content is about 44% of the mean value. The cumulative specific fission value would also be expected to vary The ratio of Pu-239 to the higher Pu isotopes is lower than that of the MHR so that, in fact, the total amount of plutonium at discharge is only somewhat lower than MHR fuel at the same burnup.

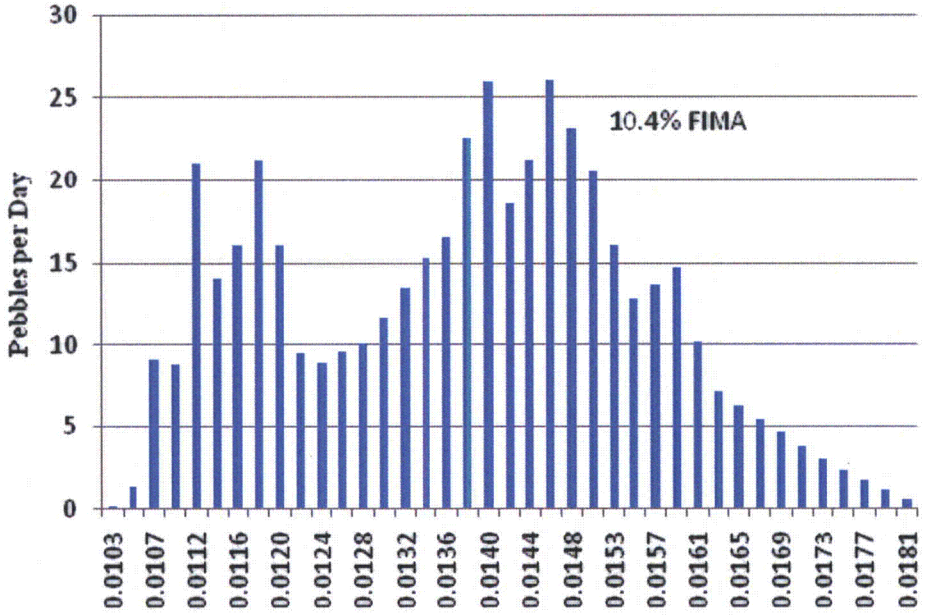


Figure 21. Specific Mass of plutonium in Discharged Pebbles (g/mass of initial U).

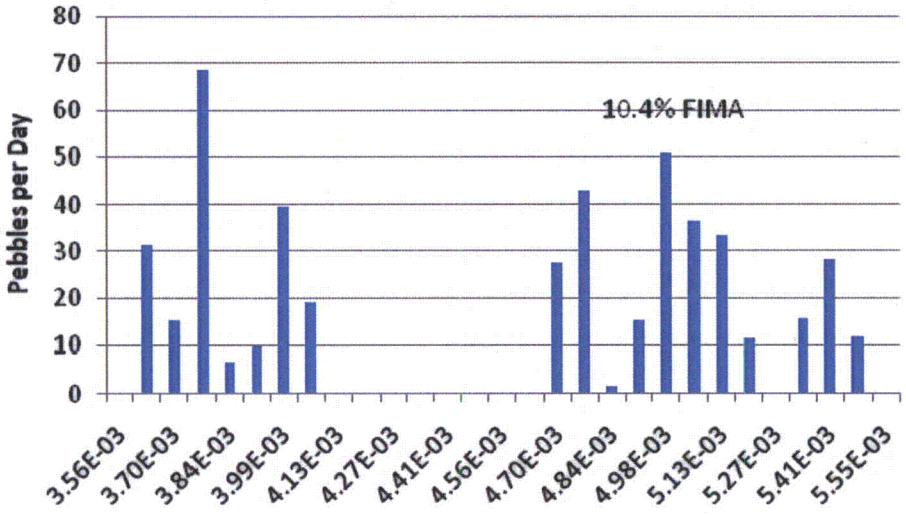


Figure 22. Specific Mass of Pu-239 in Discharged Pebbles (g/mass in initial U).

Figure 23 shows the distribution of Pu-240, the immediate capture product of Pu-239. With a little imagination, it appears to have the inverse shape of the Pu-239 curve. The Pu-241 curve (Figure 24) shows a tendency toward a double peak. Altogether, these plots indicate a complex balance between creation and destruction of the plutonium isotopes in the PBMR400 core.

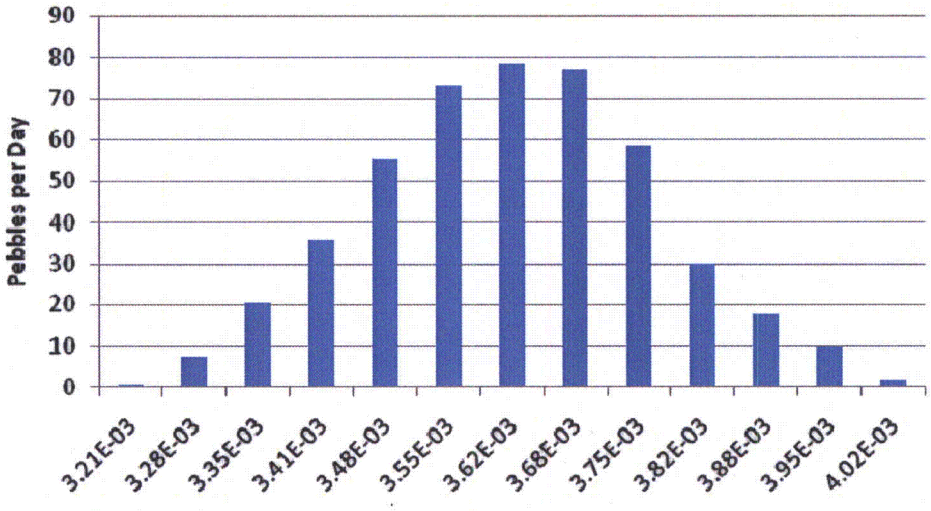


Figure 23. Specific Mass of Pu-240 in Discharged Pebbles (g/mass of initial U).

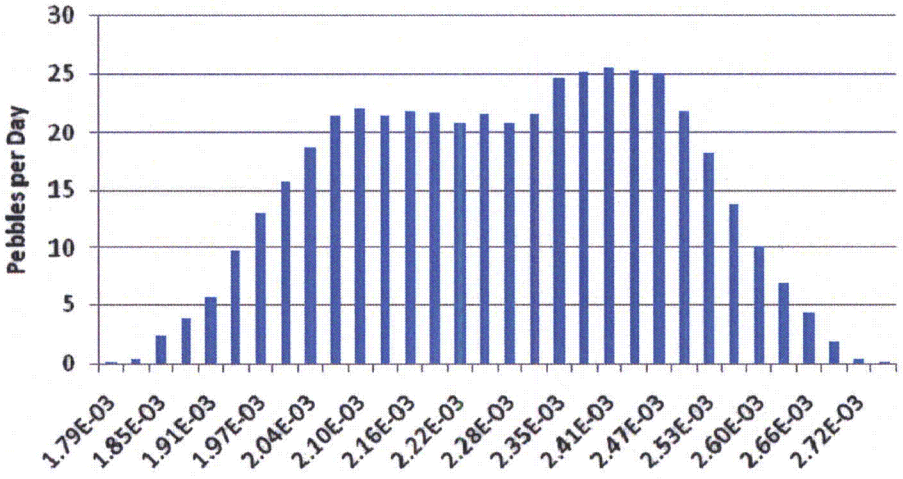


Figure 24. Specific mass of Pu-241 in discharged Pebbles (g/mass of initial U).

The variability in fissile transmutation will lead to variability in the concentration of fission products. This is illustrated in Figures 25 and 26. Figure 25 shows the distribution in the sum of the discharge concentrations of Ag-109 and Ag-110 m.

The distribution is closer to normal with a total spread of about 25% of the mean. Figure 26 shows a similar curve for the sum of the palladium isotopes (atomic masses 102,104,105,106,107,108, and 110) but with a spread between the minimum and maximum of about 33% of the mean.

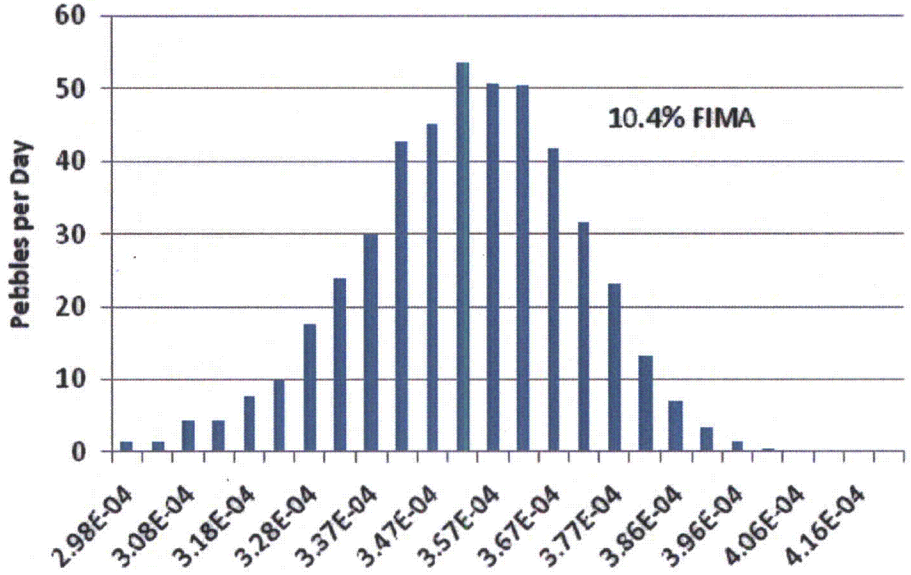


Figure 25. Specific Mass of Ag-109 + Ag-110m in Discharged Pebbles.

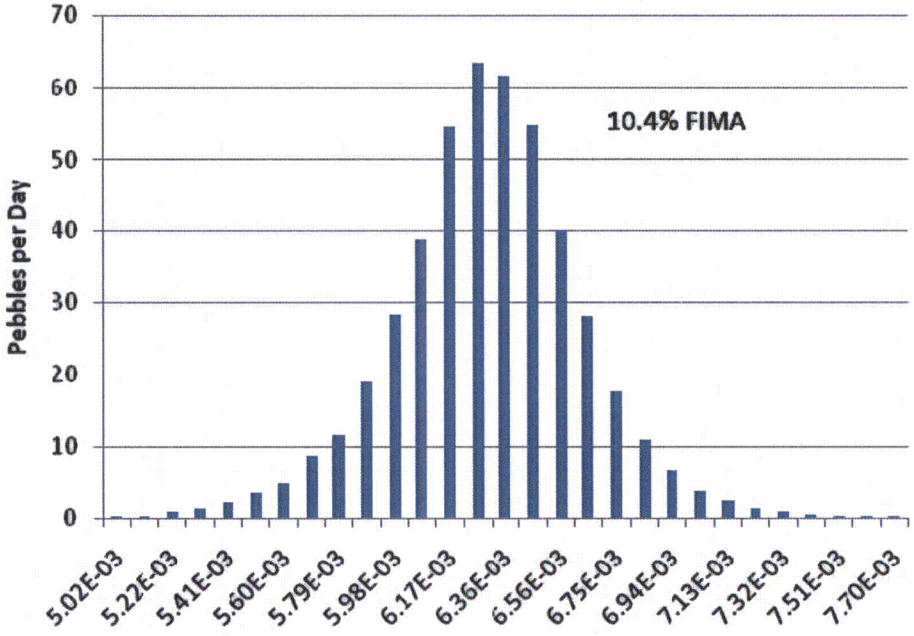


Figure 26. Specific Mass of palladium in Discharge Pebbles.

As fission products, the concentrations will be limited by the total number of fissions that occurred in the fuel and thus one can reasonably assume that the concentration in the AGR test will be higher than this prediction for PBMR400 fuel. Also, because the specific fissions for the prismatic HTGR are within 10-15% of the PBMR values, the specific mass distributions for silver and palladium

shown in these plots can be considered 1st order estimates for the prismatic core at a comparable burnup.

Even taking into account the spectral differences across the pebble bed and the expected variations in burnup, the AGR-1 test appears to be bounding in terms of fissions per gram of initial uranium. PBMR400 fuel is designed to be burned to about 97 GWD/MTU (10% FIMA) which is about half that attained in the AGR-1 test (187 GWD/MTU). Thus the concentrations of fission products generated in the AGR-1 test will be higher than that attained in the pebble bed HTGR even with the anticipated variations in the core spectra.

Some of the AGR-1 particles will undergo post-irradiation chemical analysis to yield estimates of fission product and minor actinide concentrations. This data can be used to validate the isotopic numbers cited within this study.

# 3. SUMMARY

Two questions were posed with regard to applicability of AGR-1 test data to NGNP fuel performance modeling. The first asked if radiation-enhanced effective diffusivities of fission products through the fuel compacts can be extracted from measurements of fission product concentrations taken outside of the radiation field. In this report, a method was described for estimating the contributions of different mechanisms to fission product diffusion through TRISO fuel materials using data from the AGR-1 and AGR-2 tests. From these measurements and data reduction, effective diffusion coefficients for fuel under irradiation that reflect athermal, radiation-enhanced, and intrinsic diffusion mechanisms can be obtained for use in fuel performance codes such as PARFUME.

The second question concerned the rate and total accumulation of certain fission products that are known to affect fuel performance. Specifically, are the expected concentrations attained in AGR-1 fuel comparable to those anticipated in either prismatic or pebble bed fuel under normal operating conditions. In this report, palladium and silver atom concentrations were estimated for maximum burnup AGR-1 and prismatic MHR compact fuel. The maximum burnup MHR fuel is predicted to contain approximately 49% more palladium atoms and 66% more silver atoms than the AGR-1 fuel. Although these differences are significant, the relative palladium and silver concentrations do not differ by orders of magnitude. The main reason is that the bulk of the fissions in both the MHR and AGR-1 fuel are due to U-235 fission and not plutonium. For MHR and AGR-1 fuel with lower burnups the differences are expected to be even smaller.

The average spectrum in the PBMR400 is comparable to that of the MHR, but it is expected to discharge fuel pebbles at approximately 95,000-100,000 GWD/MTU, approximately half the maximum burnup in the MHR. This is also considerably less than that attained in the AGR-1 test. The variation in the burnup of individual pebbles is a small fraction of the mean and so it is expected that the concentrations of fission products in the AGR-1 test will be higher than that predicted for pebble bed reactor fuel under all anticipated conditions.

# Appendix A
# Original Query from the Nuclear Regulatory Commission

April 20, 2010

Note to: William D. Reckley, Chief, NRO/ARP/ARB1

From: Donald E. Carlson, Senior PM, NRO/ARP/ARB1

Subject: Proposed Discussions with INL on Selected Fuel-Related Issues

As discussed, described below are two of the HTGR/NGNP fuel-related technical issues that we should try to discuss with INL at their earliest convenience, hopefully next week in Denver.

**Issue 1: Effects of different neutron energy spectra on TRISO fuel performance**

1.1. Background and general observations:

When HTGR fuel qualification irradiations are performed in material test reactors (MTRs), consideration must be given to how differences between the HTGR and MTR neutron energy spectra could lead to differences in fuel integrity and retentiveness. Such considerations generally include ensuring that the HTGR fuel design values of fast neutron fluence and total burnup are enveloped by those achieved in the MTR irradiations. However, especially for low-enriched uranium (LEU) fuels, it is also important to evaluate how the neutron spectral differences affect uranium-to-plutonium conversion factors, nuclide-specific (U-235/U-238/Pu-239/Pu-241) fission rates and burnup, and the produced inventories of chemical elements that can affect fuel performance. The following observations bear noting in this context:

- Plutonium fission generally accounts for a large and variable fraction of the total burnup in LEU fuels. For a given initial uranium enrichment and total fuel burnup, the magnitude of the plutonium fission fraction will vary with changes in the neutron energy spectrum. An HTGR spectrum may convert more uranium to plutonium than a water-cooled MTR spectrum. Furthermore, for a given inventory of Pu-239 in relation to U-235, the harder thermal neutron spectrum in an HTGR, which typically peaks near the 0.3 eV fission resonance of Pu-239, will more strongly favor Pu-239 fission over U-235 fission.

- The different fissionable nuclides (mainly U-235, U-238, Pu-239, Pu-241) that undergo fission in LEU fuel have very different yields of certain fission products that can affect TRISO fuel performance. In particular, the fission yields of silver and palladium and various rare earths are many times higher from plutonium fission than from U-235 fission. Therefore, the total production of these fission products may be more a function of plutonium burnup than total burnup.

- It is widely noted that palladium and various rare earth fission products can have deleterious effects on particle coating integrity.[1] The effects of palladium have been summarized as follows: "Fission product palladium is known to attack SiC at localized reaction sites. These interactions have been the subject of extensive study. In high burnup LEU fuels, 25 to 50x more palladium is produced than in either high burnup HEU fuels or LEU low burnup fuels because of the large fraction of fissions from plutonium that are expected at high burnup. As a result, the potential for palladium attack of the SiC could be higher in LEU high burnup fuels like that proposed for NGNP. A review of the international database shows no strong dependence on burnup or the composition of the kernel, although theoretically this could be important."[2]

- It is also widely noted that silver diffuses readily through SiC at high fuel operating temperatures. In the past, researchers have hypothesized that the cumulative effects of silver diffusion could alter the SiC grain boundaries. For example: "In the part played by silver it is not clear whether the release is determined by an independent diffusion process or whether silver and palladium first widen the SiC grain boundaries and can be regarded as precursors of SiC damage." One could further hypothesize that effects of silver diffusion on SiC grain boundaries could also increase the grain boundary diffusion of cesium.

- Initial information needed for evaluating the effects of different neutron energy spectra in MTRs versus HTGRs would include the following calculated or measured quantities as functions of total burnup and irradiation time: (a) fissions of U-235, U-238, Pu-239, and Pu-241, and (b) inventories of palladium, selected rare earth fission products, and silver.

1.2. Information needs to be discussed with INL

For (a) a reference HTGR design as well as (b) the recently completed AGR-1 and subsequent TRISO fuel irradiations in the ATR, please provide the following calculated quantities presented as functions of total burnup and irradiation time:

i. the changing inventories of fissionable nuclides that contribute significantly to total fuel burnup (e.g., U-235, U-238, Pu-239, Pu-241) and associated nuclide-specific fission rates and burnup fractions,

ii. the resulting production and inventories of chemical elements that can potentially affect TRISO fuel performance, including palladium, rare earths, and silver.

Discussion points:

The HTGR spectra and burnup calculations should be realistic rather than conservative. Note that fuel will generally reside in various HTGR core locations as it is burned, ranging from

1. R. Morris, D. Petti, D. Powers, B. Boyack, TRISO Coated Particle Fuel Phenomena Identification and Ranking Tables (PIRTs) for Fission Product Transport Due to Manufacturing, Operations, and Accidents, NUREG/CR-6844, Volumes 1-3, July 2004.
2. D. Petti, J. Maki, The Challenges Associated with High Burnup and High Temperature for UO2 TRISO Coated Particle Fuel, MIT NGNP Symposium, INL/CON-05-00038, February 2005.

the coolest positions at the top inlet to the hottest positions at the bottom outlet. The cooler HTGR spectra may tend to more closely resemble the spectra in the ATR or other water-cooled MTRs. The VHTR spectrum plot that was presented last year at Las Vegas appears be that for a very hot location at the bottom of the core.

Our initial goal is to get an order-of-magnitude estimate of the relative inventories of palladium, silver and rare earths in TRISO fuels as they are irradiated in representative HTGR spectra versus the spectra in the ATR tests. For this initial purpose, past calculations performed for pre-test design predictions of the AGR-1 irradiations should suffice to determine whether the differences at high burnups are on the order of 30 percent versus 300 percent, etc.

Can the requested information be provided by INL? If so, when? If the information will not be provided soon by INL, the NRC may chose to perform its own calculations to model the TRISO fuel burnup isotopics in the ATR irradiations. In that case, could INL provide the detailed information needed for modeling the ATR irradiations?

**Issue 2: Diffusion through intact TRISO coatings during irradiation**

Description of technical issue

Metallic fission product (e.g., cesium) release data obtained from accident heat-up simulation tests are used for predicting metallic fission product diffusion coefficients for the fuel temperatures associated with a core heat-up accident. Because these heat-up tests are conducted as part of post-irradiation testing, they do not address any diffusion-related phenomena that are present during irradiation and absent afterward. The additional use of such post-irradiation heat-up data as "margin data" for predicting fission product diffusion during irradiation at operating temperatures above those addressed by the fuel qualification irradiations could therefore be non-conservative. For example, recent experiments and atomistic simulations have suggested that lattice vacancies play an important role in both the solubility and the diffusion of cesium in SiC.[3] It is well known that neutron irradiation produces not only extended defects such as dislocation loops and voids but also temporary lattice vacancies and interstitials that disappear soon after irradiation stops.[4] These non-equilibrium vacancies and interstitials would likely increase solubility of cesium in SiC and accelerate cesium diffusion during irradiation. Post-irradiation measurements would miss this effect and thus potentially underpredict cesium diffusion during irradiation. In general, the evaluation of diffusion effects during irradiation should consider how the concentration of lattice vacancies increases with both irradiation intensity and temperature.

Discussion points

Has anyone ever measured or predicted the temporary increase in cesium diffusion through SiC that occurs during irradiation? What has been or could be done to address this?

3. T. Allen, I. Szlufarska, D. Morgan, K. Sridharan, M. Anderson, and L. Tan, University of Wisconsin, Semi-annual report to the Nuclear Regulatory Commission on the Cooperative Agreement for Research on Advanced VHTRs, January 2010.
4. W. Schilling, Properties of Frenkel defects; and L. Hobbs, F. Clinard Jr., S. Zinkle, R. Ewing, Radiation effects in ceramics, Journal of Nuclear Materials, Vol 216 (1994), Pages 45-48 and 291-321.